Stem Cell Reports
Article

ISSCR

OPEN ACCESS

DOT1L inhibition enhances pluripotency beyond acquisition of epithelial identity and without immediate suppression of the somatic transcriptome

Coral K. Wille[1] and Rupa Sridharan[1,2,*]
[1]Wisconsin Institute for Discovery, University of Wisconsin, 330 North Orchard Street, Room 2118, Madison, WI 53715, USA
[2]Department of Cell and Regenerative Biology, University of Wisconsin-Madison, Madison, WI 53705, USA
*Correspondence: rsridharan2@wisc.edu
https://doi.org/10.1016/j.stemcr.2021.12.004

SUMMARY

Inhibiting the histone 3 lysine 79 (H3K79) methyltransferase, disruptor of telomeric silencing 1-like (DOT1L), increases the efficiency of reprogramming somatic cells to induced pluripotent stem cells (iPSCs). Here, we find that, despite the enrichment of H3K79 methylation on thousands of actively transcribed genes in somatic cells, DOT1L inhibition (DOT1Li) does not immediately cause the shutdown of the somatic transcriptional profile to enable transition to pluripotency. Contrary to the prevalent view, DOT1Li promotes iPSC generation beyond the mesenchymal to epithelial transition and even from already epithelial cell types. DOT1Li is most potent at the midpoint of reprogramming in part by repressing *Nfix* that persists at late stages of reprogramming. Importantly, regulation of single genes cannot substitute for DOT1Li, demonstrating that H3K79 methylation has pleiotropic effects in maintaining cell identity.

INTRODUCTION

Differential gene expression allows for functional diversity that translates to tissue specialization in multicellular organisms. In response to signaling and spatial cues, transcription factors engage with the epigenome to culminate in gene expression patterns that establish cell identity (Kelsey et al., 2017). The abundance of specific epigenetic modifications changes dynamically during development, right from the formation of the zygote (Dang-Nguyen and Torres-Padilla, 2015; Smith and Meissner, 2013). Fertilization of an oocyte triggers a decrease in histone 3 lysine (K) 79 dimethylation (H3K79me2) independent of genome replication (Ooga et al., 2008). H3K79me2 levels remain low during the pre-implantation phase until the blastocyst stage (Ooga et al., 2008). H3K79me2 is the most differential histone modification between somatic cells and embryonic stem cells (ESCs) that are derived from the blastocyst (Sridharan et al., 2013).

Disruptor of telomeric silencing 1-like (DOT1L) is the sole methyltransferase that performs all levels (me1, me2, and me3) of H3K79 methylation (called H3K79me henceforth; Black et al., 2012). *Dot1l* knockout (KO) mice are embryonic lethal between days 9.5 and 13.5, demonstrating the importance of H3K79me in development (Feng et al., 2010; Jones et al., 2008). *Dot1l* KO results in disorganized yolk sacs containing primitive erythrocytes. DOT1L is also necessary for development of the heart (Nguyen and Zhang, 2011), cerebral cortex (Franz et al., 2019), and chondrocytes (Castaño Betancourt et al., 2012) and normal $CD8^+$ T cell differentiation (Kwesi-Maliepaard et al., 2020). H3K79me is not required for pluripotency, as ESCs continue to self-renew in the absence of DOT1L or DOT1L catalytic activity (Barry et al., 2009; Cao et al., 2020; Jones et al., 2008). We and others have shown that DOT1L is a barrier for transcription-factor-mediated reprogramming to induced pluripotent stem cells (iPSCs) from mouse neural stem cells and human fibroblasts (Jackson et al., 2016; Onder et al., 2012).

Collectively, these phenotypes provide evidence for the importance of DOT1L in cell fate determination; however, the function of H3K79me in mammals has remained elusive. H3K79me2 is enriched on the bodies of rapidly elongating genes (Duffy et al., 2018; Veloso et al., 2014), implicating the modification as a positive regulator of transcription. In acute leukemia, fusion proteins between mixed-lineage leukemia (MLL) and numerous DOT1L-associated proteins (ENL, AF9, and AF10) frequently drive oncogenesis (Mohan et al., 2010). MLL target genes, such as the *HOXA* cluster, are upregulated concurrent with the corresponding locus becoming H3K79 methylated as DOT1L is mislocalized via the MLL-DOT1L-interacting fusion protein. In contrast, H3K79me enrichment directly downregulates the expression of the epithelial sodium channel gene in mouse cells (Zhang et al., 2006), confounding the role of DOT1L in transcription.

Here, we use the dynamic system of somatic cell reprogramming from mouse embryonic fibroblasts (MEFs) to iPSCs to investigate DOT1L function in maintaining cell identity. We find that DOT1L inhibition enhances MEF pluripotency acquisition throughout the process but acts most potently at mid-reprogramming. This dramatic increase in reprogramming is accompanied by few steady-state transcriptional changes. Previous studies have reported that DOT1L inhibition (DOT1Li) enhances reprogramming by facilitating the mesenchymal to epithelial transition (MET) that occurs when reprogramming fibroblasts (Apostolou and Hochedlinger, 2013; Onder et al., 2012). However, with orthogonal

experiments, such as expressing *Cdh1* during reprogramming, testing cells after MET, and reprogramming keratinocytes that are already epithelial, we conclusively demonstrate that DOT1Li enhances pluripotency far beyond the transition to the epithelial identity. Using a small interfering RNA (siRNA) screen, we identify *Nfix*, which remains highly expressed throughout reprogramming, as a regulator that collaborates with DOT1L to reduce iPSC formation. Therefore, DOT1Li increases pluripotency acquisition in part by preventing upregulation of reprogramming-associated genes, which contributes to the continued requirement of DOT1Li into the mid-phase of reprogramming. DOT1Li does not immediately switch off the somatic transcriptome to favor pluripotency and functions through pleiotropic effects.

RESULTS

DOT1L enzymatic activity is a barrier for reprogramming

We used a secondary reprogramming system to assess how DOT1L affects MEF pluripotency acquisition. MEFs isolated from mice that contain *Oct4*, *Sox2*, *Klf4*, and *c-Myc* (OSKM) (Sridharan et al., 2013) under a doxycycline-inducible promoter were reprogrammed with *Dot1l* knockdown using siRNA. With depletion of just half of the *Dot1l* transcript (Figure S1A), reprogramming was increased 2-fold (Figure 1A). Because DOT1L protein can function independent of catalytic activity (Cao et al., 2020), we next inhibited DOT1L using two extremely specific small molecules with no reported off-target effects (Figure 1B; Daigle et al., 2013; Kaniskan et al., 2018; Yu et al., 2012). SGC0946, hereafter called DOT1Li, disrupts DOT1L interaction with S-adenosyl methionine (SAM) by inducing a conformational change and is 10-fold more potent than the first-generation DOT1Li inhibitor, EPZ004777 (Yu et al., 2012). Both EPZ004777 (Nassa et al., 2019) and SGC0946 (Wu et al., 2021) were recently shown to reduce DOT1L occupancy at target genes. EPZ5676, known as pinometostat, is a highly selective DOT1L inhibitor that also prevents SAM interaction and has entered clinical trials (Campbell et al., 2017). Both chemical inhibitors decreased H3K79me2 with similar kinetics compared with control (Figure 1B) and comparably increased reprogramming of MEFs as measured by NANOG expression (Figures 1C, S1B, and S1C). Importantly, DOT1Li produced at least 9-fold more *bona fide* pluripotent colonies that maintained NANOG expression after removal of transgene expression by withdrawal of doxycycline (Figures 1C, S1B, and S1C, right). Similar concordance of increased reprogramming efficiency from human somatic cells has been reported when using RNAi-mediated depletion and catalytic inhibition with EPZ00477 (Onder et al., 2012).

To determine the temporal requirement for DOT1Li to enhance reprogramming, we performed a 6-day time course (Figure 1D, left). When reprogramming populations were exposed to DOT1Li in 2-day intervals, the greatest increase in reprogramming was observed with treatment between days 2 and 4 (Figure 1D, blue bars). Removing DOT1Li between days 2 and 4 resulted in fewer NANOG-positive colonies compared with 4 days of continuous DOT1Li treatment either early or late in reprogramming (Figure 1D, red bars). The greatest number of NANOG$^+$ colonies formed when DOT1L was inhibited throughout reprogramming. Thus, DOT1L activity is a barrier to reprogramming throughout the conversion process but has the greatest effect in the intermediate phase.

Loss of H3K79me during reprogramming results in few steady-state transcriptional changes

To elucidate how loss of H3K79me enhances iPSC generation, the starting MEFs, reprogramming populations on days 2 and 4, and ESCs were transcriptionally profiled using RNA sequencing (RNA-seq). Independent experiment replicate samples collected on day 4 were treated continuously with DOT1Li, treated "early" from day 0 to 2, treated "mid" from day 2 to 4, or treated continuously with vehicle control (Figures S1D and S1E) to capture how DOT1Li specifically increases mid reprogramming (Figure 1D). Continuous DOT1Li for 4 days resulted in the most transcriptional alterations compared with early or mid treatment (Figures 1E, S1G, and S1H). Three hundred fifty-two genes were differentially expressed (Figure 1E; experimental procedures), with 10-fold more genes upregulated than downregulated. The majority of differentially expressed (DE) genes had a modest change in expression (Figure 1F). This low-magnitude change in expression occurred in genes with low levels of absolute expression (Figure 1G). Mid treatment from day 2 to 4 with DOT1Li yielded the next highest number of changes, with 125 upregulated genes and 2 downregulated genes (Figure S1H), followed by day 2 DOT1Li (51 upregulated and 1 downregulated; Figure S1F). Removal of DOT1Li after 2 days (early treatment) resulted in only nine DE genes (Figure S1G). Accordingly, early treatment clustered closest with day 4 control-treated replicates (Figure S1D). At every time point, a far greater number of upregulated than downregulated genes were DE.

H3K79me2 is enriched on numerous genes, yet few change their steady-state mRNA levels

DOT1Li could promote iPSC generation by erasing the somatic program, enhancing pluripotent gene expression, or a combination of the two. To distinguish between these possibilities, significantly DE genes from all time points

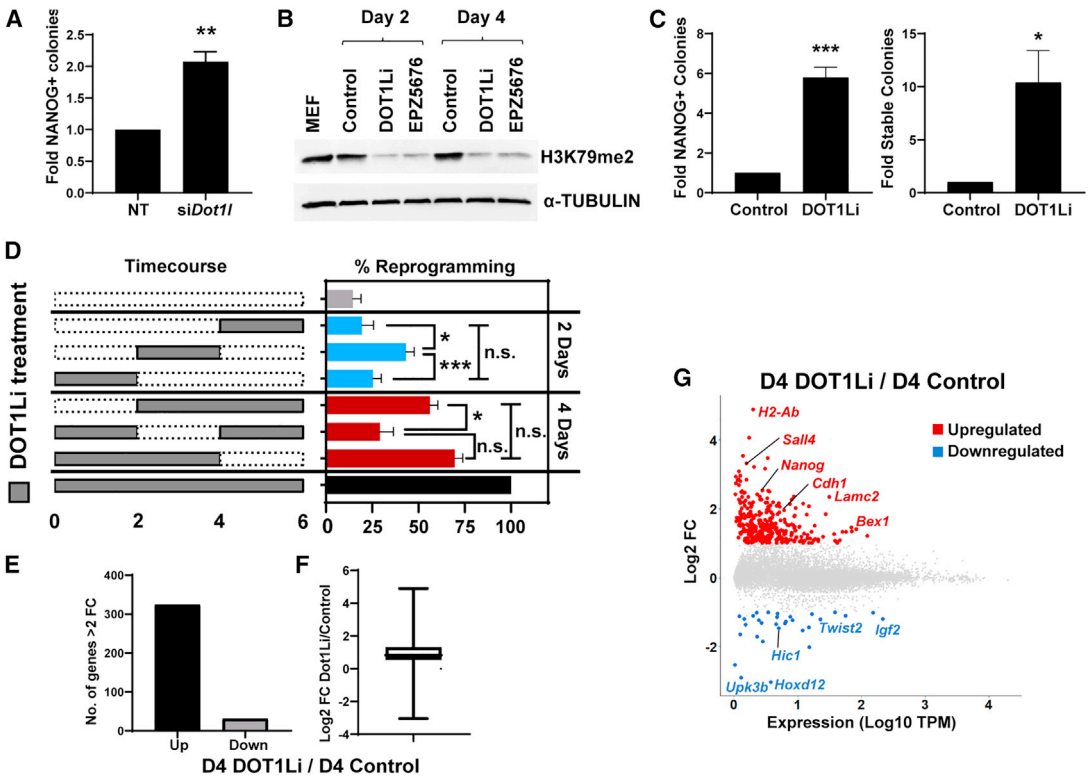

Figure 1. Loss of H3K79me during reprogramming results in few steady-state transcriptional changes

(A) Reprogramming efficiency of MEFs treated with control non-targeting (NT) siRNA or depleted for *Dot1l* (si*Dot1l*). Error bars represent the SEM of three independent experiment replicates, each composed of two or three technical replicates. Colonies obtained in NT were set to 1. **p < 0.01 by unpaired t test.

(B) Immunoblot of H3K79me2 and TUBULIN loading control of reprogramming cells on day 2 or 4 treated with control DMSO, SGC0946 (DOT1Li), or EPZ5676.

(C) NANOG$^+$ colonies obtained on days 6 to 7 after induction of OSKM in MEFs (left) and stable (NANOG$^+$/DPPA4$^+$) colonies 2–4 days post-doxycycline (dox) and drug removal (right) with control or DOT1Li. Colonies obtained in control treatment were set to 1. Error bars represent the SEM of three independent experiment replicates, each composed of two or three technical replicates. ***p < 0.001 and *p < 0.05 by unpaired t test.

(D) (Left) Scheme of exposure to DOT1Li (gray boxes) or control (dotted boxes). (Right) Number of NANOG$^+$ colonies on day 6 is shown. Colonies obtained in day 0–6 continuous DOT1Li treatment were set to 100% (black bar). Error bars represent the SEM of three independent experiment replicates, each consisting of two or three technical replicates. Each duration of DOT1Li treatment, 2 days (blue bars) or 4 days (red bars), was assessed by one-way ANOVA. Significance was calculated *post hoc* with the Tukey test: ***p < 0.001, *p < 0.05, and not significant (n.s.), p > 0.05.

(E) Number of genes upregulated or downregulated by a more than 2-fold change (FC) with a posterior probability of differential expression greater than 0.95 determined by EBSeq in day 4 DOT1Li versus day 4 control.

(F) Boxplot of log2 FC of all genes with a posterior probability of differential expression greater than 0.95 in day 4 DOT1Li relative to day 4 control.

(G) Log10 of the averaged transcripts per million (TPM) of day 4 DOT1Li and 4 control versus log2 FC of all genes. More than 2-fold upregulated is indicated in red and downregulated indicated in blue.

See also Figure S1.

(n = 438; "DOT1Li-DE") were compared with the change in gene expression in ESCs versus MEFs. While about 50% of DOT1Li-downregulated genes were also decreased in ESCs, far fewer of the DOT1Li-upregulated genes were upregulated in ESCs, suggesting that most of the steady-state transcriptional change is aberrant to that observed in ESCs (Figure 2A).

We then asked whether the transcriptional changes were correlated with the presence of H3K79 methylation. Chromatin immunoprecipitation sequencing (ChIP-seq) of H3K79me2 in MEFs derived from the same reprogrammable mouse line and ESCs was analyzed (Figure 2B; Chronis et al., 2017). As expected, highly expressed genes were enriched for

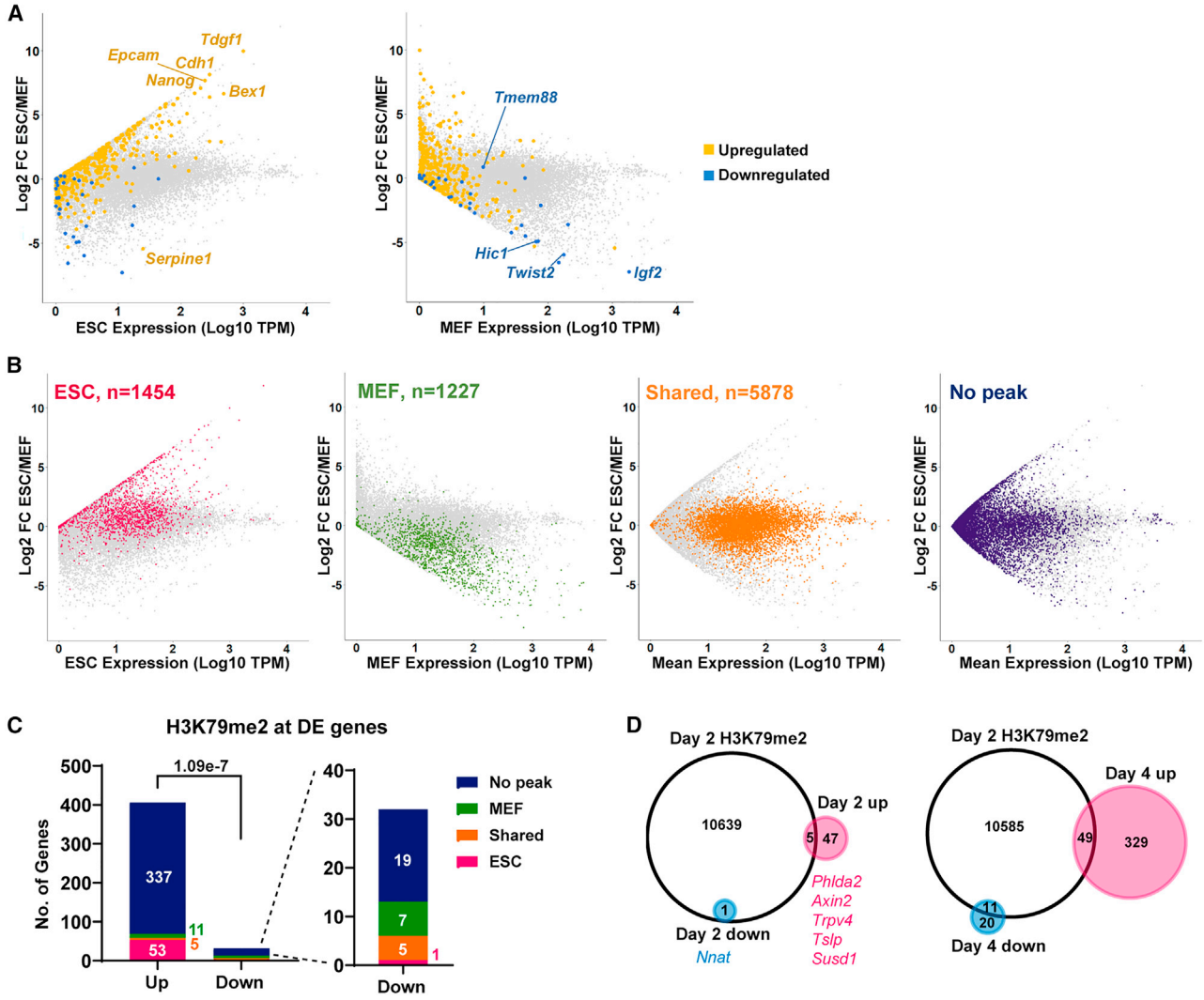

Figure 2. H3K79me2 is enriched on numerous genes, yet few change transcriptionally in steady-state mRNA levels

(A) Genes upregulated (gold) or downregulated (blue) by DOT1Li treatment at any time point relative to the matched control (DOT1Li-DE list) plotted on expression calculated as log10 of ESC TPM (left) or MEF TPM (right) versus log2 FC in ESCs relative to MEFs.

(B) Genes with H3K79me2 called peaks in ESCs (red), in MEFs (green), shared in both cell types (orange), or with no peak (purple) were plotted onto the indicated expression calculated as log10 TPM versus log2 FC in ESCs relative to MEFs. H3K79me2 location data were analyzed from GEO: GSE90895 (Chronis et al., 2017).

(C) Bar graph of H3K79me2 called peaks at DOT1Li-DE genes. Significance calculated by Fisher's exact test is shown.

(D) Overlap of genes with an H3K79me2 peak on day 2 of reprogramming (Chronis et al., 2017) with DE genes at the indicated time points. See also Figure S2.

H3K79me2 in both MEFs and ESCs. Genes with "shared peaks" were highly expressed and predominantly housekeeping genes (Figure S2A). In addition, many low-expressed genes did not have a significant H3K79me2 peak, yet a subset of these genes were DE in ESCs versus MEFs (Figure 2B, "no peak").

The majority of DE genes did not have an H3K79me2 peak (Figures 2C, S2B, and S2C). Thirteen percent of upregulated genes had a peak in ESCs, while only 2.7% had a peak in MEFs, and 1.2% had a shared peak (Figure 2C). Only 22% of downregulated genes had a peak in MEFs, 16% had a shared peak, and 1 gene had a peak in ESCs (Figure 2C). To capture whether transient gain in H3K79me2 during reprogramming affects gene expression, DE genes at day 2 or 4 of reprogramming overlapped with genes modified by H3K79me2 48 h after OSKM induction. Very few DE genes contained an H3K79me2 peak during reprogramming, and the majority were upregulated (Figure 2D).

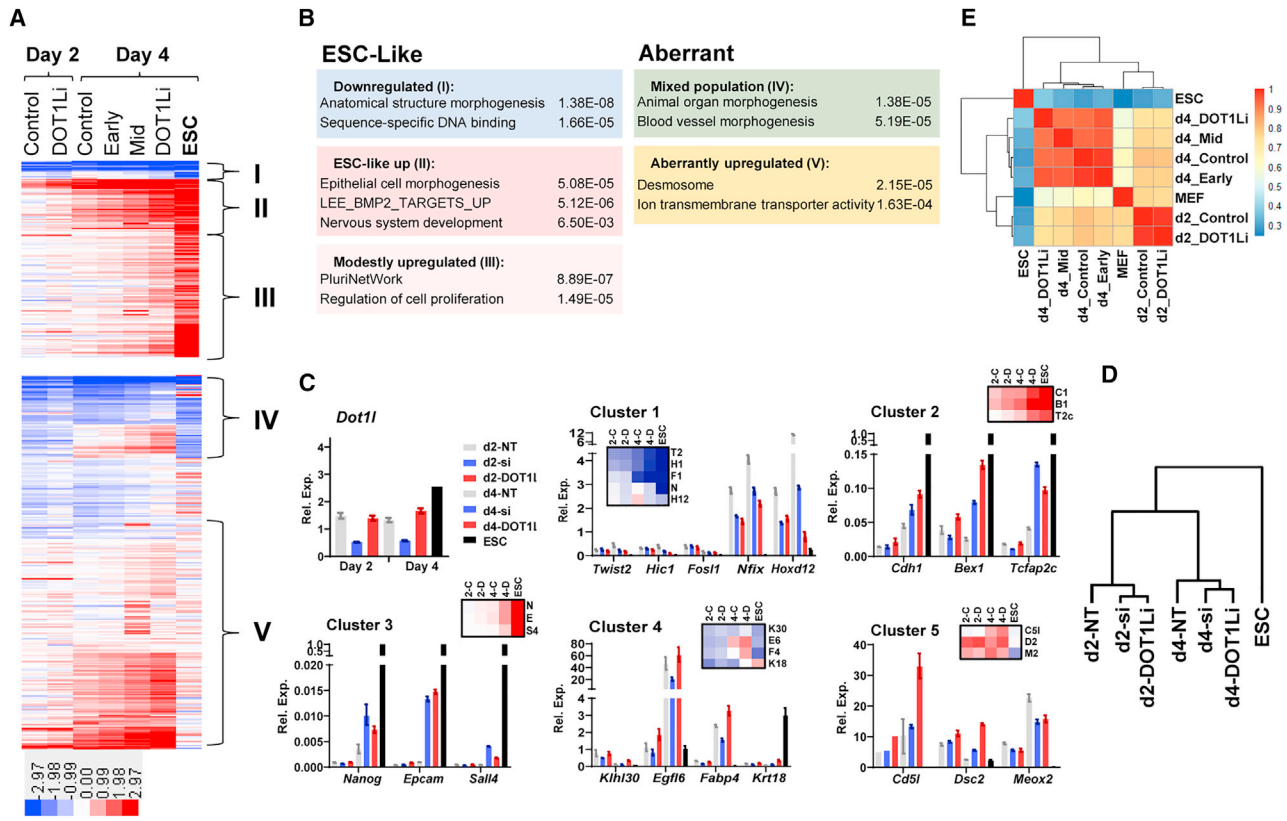

Figure 3. DOT1L inhibition leads to transcriptional changes not observed in MEFs or ESCs

(A) k-means clustering of DOT1Li-DE genes organized based on transcriptional change in ESCs relative to MEFs. Heatmap intensity indicates log2 FC TPM relative to MEF for each sample.

(B) Representative gene ontology categories for each cluster. The most enriched categories containing unique sets of genes are displayed (HOMER).

(C) qPCR validation of select genes from every cluster in non-targeting control (NT) treated with control DMSO, si*Dot1l* (si), and DOT1Li. Normalized expression in MEFs was set to 1 for *Dot1l* and clusters 1, 4, and 5. Normalized expression in ESCs was set to 1 for clusters 2 and 3. All samples shown are from day 2 (left) to day 4 (right). Insets: zoomed-in RNA-seq heatmaps of assessed genes in control (C), DOT1Li (D), and ESCs at day 2 (2) and day 4 (4). Genes are abbreviated as first initial and number.

(D) Hierarchical clustering of relative expression of tested genes (C).

(E) Spearman correlation of DOT1Li-DE gene TPM across all samples.

See also Figure S3.

DOT1L inhibition leads to transcriptional changes not observed in MEFs or ESCs

To ascertain the functional role of DOT1Li during reprogramming irrespective of time point, all DOT1Li-DE genes were clustered and visualized on a heatmap relative to their expression in MEFs (Figure 3A). Genes in clusters I–III were changed by DOT1Li to resemble ESC-like expression and included transcription factors involved in structure morphogenesis, epithelium, and proliferation genes (Figures 3A, 3B, and S3A). In contrast to genes in clusters I–III, the majority of genes (clusters IV and V) do not resemble the transcriptional profile of ESCs relative to MEFs (Figure 3A). Genes in cluster IV (n = 60) are a mixed population of aberrantly upregulated genes, or their downregulation is prevented by DOT1Li (Figures 3A and S3A) and they are not functionally related. Cluster V (n = 160) contains genes that are upregulated by DOT1Li treatment yet are largely unchanged in ESCs relative to MEFs (Figures 3A and S3A) that function in transmembrane signaling (Figure 3B).

As an independent validation of these trends in transcriptional profile, we verified the expression changes in an siRNA-mediated depletion of *Dot1l* over a 6-day time course. Samples were collected on day 2 and day 4 and showed a greater than 2-fold decrease in *Dot1l* expression (Figure 3C). We selected at least three genes in each cluster that represented varying levels of change on day 2 and day 4 by DOT1Li (Figure 3C, inset). The results obtained from

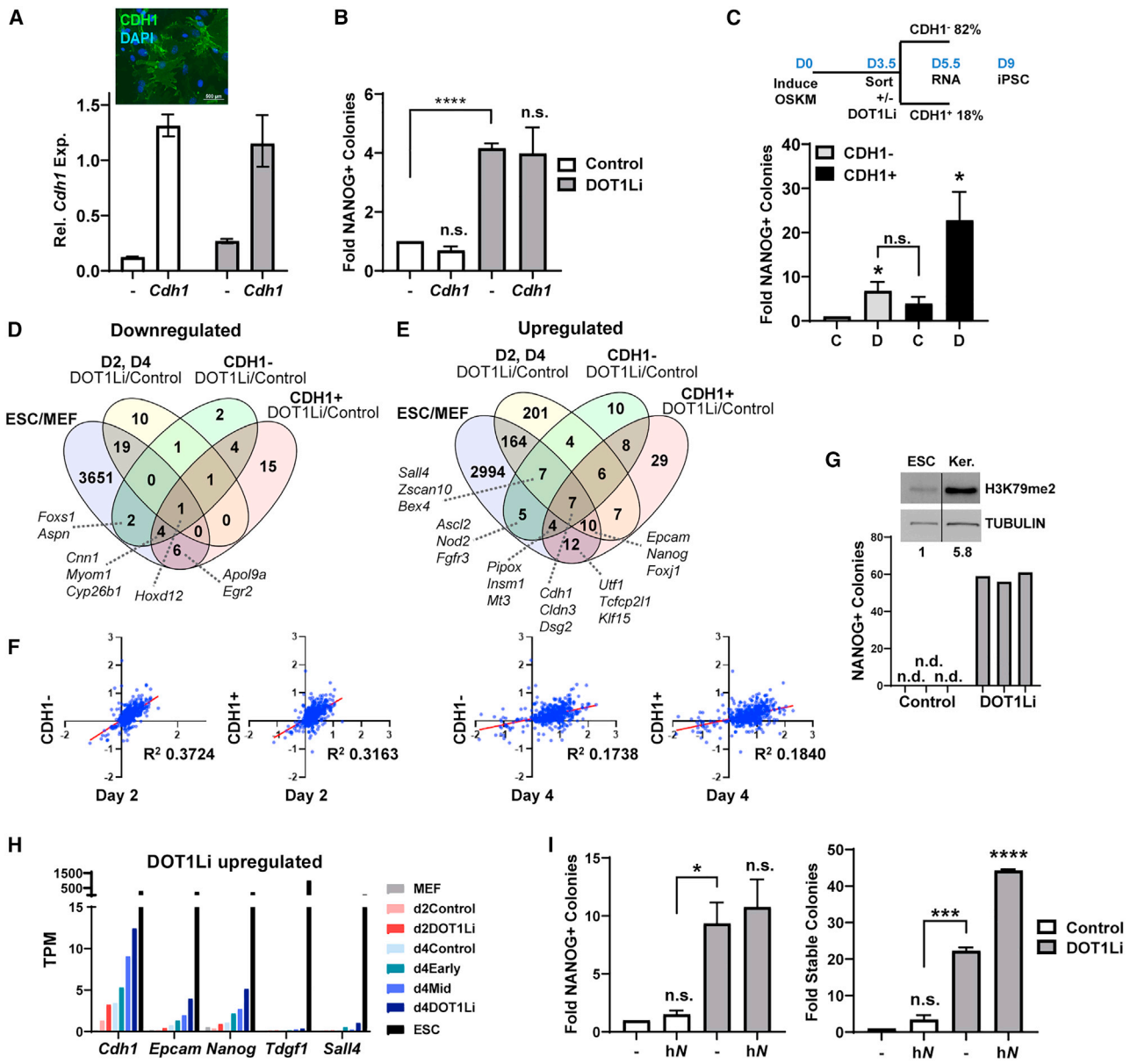

Figure 4. Inhibition of DOT1L enhances reprogramming of epithelial cells

(A) (Top) CDH1 immunofluorescence on day 4 of reprogramming of *Cdh1*-transduced cells. Scale bar represents 500 μm. (Bottom) Relative *Cdh1* expression measured on day 3 of reprogramming is shown. ESCs are set to 1. Cells were treated with control (white bars) or DOT1Li (gray bars).

(B) Fold NANOG$^+$ colonies of empty-vector- (–) or *Cdh1*-transduced cells, treated with control (white bars) or DOT1Li (gray bars). Empty-vector-transduced cells treated with control are set to 1. Error bars represent the SEM of three independent experiment replicates, each consisting of two technical replicates. ****$p < 0.0001$ and n.s., $p > 0.05$, by unpaired t test.

(C) Reprogramming scheme (top): cells were grown for 3 days in KnockOut serum replacement (KSR)-containing medium to accelerate CDH1 expression. On day 3.5, cells were sorted with flow cytometry for CDH1 surface expression, followed by DOT1Li or control treatment. RNA-seq samples were collected at day 5.5, and reprogramming was evaluated on days 8 to 9. (Bottom) NANOG$^+$ colony formation of CDH1- sorted cells treated with DOT1Li (D) or control (C) is shown. Error bars represent the SEM of three independent experiment replicates, each consisting of two or three technical replicates. *$p < 0.05$ and n.s., $p > 0.05$, by unpaired t test.

(D) Overlap of 1.5-FC DOT1Li downregulated genes in CDH1$^-$ and CDH1$^+$ cells with the downregulated genes from all time points of the DOT1Li time course (2-FC; Figure 3A) and genes downregulated in ESCs relative to MEFs (2-FC). A selection of genes is displayed.

(legend continued on next page)

the genetic knockdown cluster with DOT1L catalytic inhibition (Figure 3D). Another study using the first-generation EPZ004777 inhibitor and sh*DOT1L* in breast cancer lines found a large overlap in gene-expression changes between the two methods of depleting DOT1L function (Nassa et al., 2019). However, it remains possible that some of the transcriptional alterations that we observe are due to off-target effects of the small-molecule DOT1Li.

Although the changes in clusters I–III (Figure 3A) position DOT1Li-treated cells closer to pluripotency acquisition than control-treated cells, Spearman correlation of DOT1Li-DE gene expression shows that all time points more closely resemble MEFs than ESCs (Figure 3E). Both day 2 samples cluster together and are more correlated to day 4 control compared with other day 4 samples, suggesting day 4 control treatment is kinetically behind the other DOT1Li treatments. Because there are few transcriptional alterations, all day 4 samples cluster closely together (Figure 3E). Of the day 4 samples, day 4 early (d0–2) and day 4 control treatments are most highly correlated, explaining why a removal of DOT1Li on day 2 of reprogramming barely increases NANOG$^+$ colony formation relative to control treatment (Figure 1D).

To determine how the clusters may be regulated, we performed motif analysis and found that cluster III and, to a lesser extent, cluster II were enriched for E-boxes that can be bound by a cadre of proteins, depending on the motif context (Figure S3B). Mesenchymal E-box binding genes that repress expression are not DE by DOT1Li, with the exception of *Twist2*, which is 2-fold downregulated on day 4 with constant DOT1Li inhibition (Figure S3C). Of note, DOT1Li inhibition also activates *Mycn* (2.7-fold in day 4 DOT1Li) that binds E-boxes to promote gene activity. Thus, the balance of these two proteins may be responsible for the modest increase in expression of cluster III, which is much more significantly enriched for E-boxes compared with cluster II (Figure S3B). Cluster IV is enriched for TCF7 motifs, a transcriptional activator, which is upregulated by DOT1Li treatment. Finally, cluster V is enriched for HOXD12 and HIC1 motifs, both transcriptional regulators downregulated by DOT1Li treatment.

Thus, DOT1Li may promote development of reprogramming intermediates expressing lineage genes (Polo et al., 2012) due to subtle changes in transcription factor levels. However, as the two clusters that most resemble ESCs (I and II) are devoid of motifs bound significantly by any of the DOT1Li DE genes, it is unlikely that DOT1L regulates pluripotency acquisition through such intermediates.

Inhibition of DOT1L enhances reprogramming of epithelial cells

To investigate whether individual genes in the upregulated cohort could replace DOT1Li, we first examined the epithelial genes. MET is an early phase of reprogramming when starting with MEFs (Apostolou and Hochedlinger, 2013). Cluster II genes (Figure 3A) that were most similar in their expression changes to ESCs (Figure S3A) are enriched for epithelial genes and E-box motifs (Figure S3B). We introduced *Cdh1*, which has previously been shown to be required for pluripotency (Chen et al., 2010; Hawkins et al., 2012), into reprogrammable MEFs using a lentivirus to achieve expression comparable to that in ESCs (Figure 4A). Although CDH1 was detected at the cell surface (Figure 4A), it did not enhance MEF reprogramming (Figure 4B). It is important to note that exogenous *Cdh1* expression was incapable of causing mesenchymal gene downregulation (Figure S4A). This result supports the notion that mesenchymal gene downregulation and *Cdh1* upregulation are regulated independent of each other from our co-expression analysis of single-cell (sc) RNA-seq data, where we found that reprogramming cells can simultaneously express genes from both programs (Tran et al., 2019). Given that expression of *Cdh1* alone could not replace DOT1Li function (Figure 4B), we assessed how reduction of H3K79me affects reprogramming of cells that are already epithelial. Reprogramming MEFs were sorted on day 3.5 post-OSKM induction for cell-surface CDH1 expression (Figure 4C) to a level similar to that of ESCs (Figure S4B). Reprogramming of the CDH1$^-$ and CDH1$^+$ sorted cells was then continued in the presence of DOT1Li. Interestingly, reprogramming of both populations of cells was increased

(E) Overlap of 1.5-FC DOT1Li upregulated genes in CDH1$^-$ and CDH1$^+$ cells with the upregulated genes from all time points of the DOT1Li time course (2-FC; Figure 3A) and genes upregulated in ESCs relative to MEFs (2-FC). A selection of genes is displayed.
(F) Scatterplot of log2 FC TPM of DOT1Li versus matched control, of the indicated time course (Figure 1) x axis, and CDH1 sort (Figure 4) y axis RNA-seq samples at DOT1Li-DE genes.
(G) NANOG$^+$ colonies on day 8 of keratinocyte reprogramming, treated with DOT1Li or control. Bars represent technical replicates. n.d., not detected. Inset: immunoblot of H3K79me2 and TUBULIN loading control in ESCs and keratinocytes (Ker.) is shown.
(H) Expression (TPM) bar graph of DOT1Li upregulated reprogramming factors.
(I) Cells transduced with vector control (–) or human *NANOG* (h*N*), treated with control (white bars) or DOT1Li (gray bars). (Left) NANOG$^+$ colonies during reprogramming are shown. (Right) Stable colonies post-dox removal are shown. Colonies obtained in vector control are set to 1. Error bars represent the SEM of three independent experiment replicates, each consisting of two or three technical replicates. ****$p < 0.0001$, ***$p < 0.001$, *$p < 0.05$, and n.s., $p > 0.05$, by unpaired t test.
See also Figure S4.

to similar extents (6.8-fold) when exposed to DOT1Li (Figure 4C), indicating a response beyond the upregulation of the epithelial program.

To identify a transcriptional response after epithelial upregulation, we profiled the gene expression of CDH1$^-$ and CDH1$^+$ populations with DOT1Li. Independent experiment replicate transcriptional data from these sorted populations were highly reproducible (Figure S4C) and clustered with one another rather than with MEFs or ESCs (Figure S4D). Similar to the results from the unsorted time course (Figures 1 and 3), more genes were upregulated than downregulated by DOT1Li in both CDH1$^-$ and CDH1$^+$ populations. *Hoxd12* was the only commonly downregulated gene in CDH1$^-$, CDH1$^+$, DOT1Li-DE days 2 and 4, and ESCs relative to MEFs (Figure 4D). Upregulated genes that were altered in the same direction as their expression in ESCs (Figure 4E) were enriched for the functional categories of stem cell population maintenance and epithelial cell development. The changes mediated by DOT1Li in unsorted populations were positively correlated with those in CDH1-sorted populations (Figure 4F). Interestingly, the changes in CDH1$^-$ cells more closely resemble day 2 of the unsorted time course, whereas the CDH1$^+$ cells are comparatively more correlated to day 4 alterations (Figure 4F). Indeed, irrespective of the status of CDH1 expression in the sorted population, addition of DOT1Li further enhances the expression of pluripotent genes, such as *Nanog*, albeit to a much lower extent than in ESCs (Figure S4E).

CDH1 is an important, but not the sole, determinant of epithelial identity. Given that DOT1Li increased reprogramming from MEFs that overexpressed or were induced to express CDH1, we next investigated the effect of DOT1L on an epithelial cell type. Keratinocytes are epithelial and, despite not having to undergo MET (Li et al., 2010; Samavarchi-Tehrani et al., 2010), still reprogram poorly compared with MEFs (Nefzger et al., 2017). We isolated keratinocytes from reprogrammable mice and confirmed that they express similar levels of CDH1 on their surface compared with ESCs (Figure S4F). Because our mass spectrometry comparison of global histone modification levels was from MEFs (Sridharan et al., 2013), we performed an immunoblot for H3K79me2. Keratinocytes had over 5-fold more H3K79me2 globally than ESCs (Figure 4G, inset), confirming that high levels of this modification are a common feature of somatic cells. DOT1Li applied during keratinocyte reprogramming increased both the efficiency and the kinetics with the appearance of tens of NANOG$^+$ colonies by day 8 of reprogramming (Figure 4G). No colonies were obtained in the control at this time point, likely due to their lower reprogramming efficiency compared with MEFs (Nefzger et al., 2017). Thus, DOT1Li promotes pluripotency beyond the upregulation of epithelial identity.

We next assessed whether DOT1Li increases reprogramming through upregulation of pluripotency factors. In our previous analysis of single-cell transcriptomic analysis, we found that the co-expression of a quartet of genes, *Nanog*, *Sall4*, *Tdgf1*, and *Epcam*, within the same cell predicted a more homogeneous transition to an iPSC state (Tran et al., 2019). DOT1Li upregulated the same genes but to a much smaller magnitude than that in ESCs (Figure 4H). We introduced exogenous human NANOG (Figures S4G and S4H) and found that it enhanced transgene independence in the presence of DOT1Li (Figure 4I). Thus, DOT1Li does not increase reprogramming through *Nanog* upregulation but collaborates with NANOG specifically to maintain pluripotent colonies.

To identify whether any other DOT1Li DE genes regulate pluripotency acquisition, they were overlapped with genes identified in a large short hairpin RNA (shRNA) screen starting with the same OSKM-inducible secondary MEF system (Borkent et al., 2016). Among the genes that affected reprogramming more than 2-fold from the screen (~2,300 genes), only 10 overlapped. However, seven barrier genes were upregulated and three enhancers were downregulated by DOT1Li, in the opposite direction of pluripotency promotion (Figure S4I). Thus, the DOT1Li-mediated increase in reprogramming is unlikely to be replaced by upregulating single-gene expression. In addition, DOT1Li treatment does not increase cellular proliferation (Figure S4J) or cause changes in the cell cycle (Figures S4K and S4L), indicating that it does not enhance pluripotency by increased cell number.

Inhibition of DOT1L enhances reprogramming beyond modulation of single genes

Because DOT1Li did not change the entire transcriptional landscape either away from a somatic program or toward a pluripotency program, we used a candidate approach to screen DOT1Li-DE genes for their contribution to pluripotency acquisition. As a higher percentage of downregulated genes were modified by H3K79me2 (Figures 2C and S3D), and DOT1L has previously been reported as a barrier to reprogramming by maintaining fibroblast gene transcription (Onder et al., 2012), we comprehensively ranked DOT1Li directly downregulated genes (Figure 5A, step 1). Among the DOT1Li genes that were downregulated in ESCs versus MEFs (step 2), we filtered those that had a significant H3K79me2 peak in MEFs or 48-h post-OSKM induction (step 3) that is reduced in ESCs (step 4; Figure 5B). A change in gene expression levels between MEFs and ESCs could occur in every single cell of the starting population or could reflect a population average. We have previously performed scRNA-seq of MEFs, ESCs, and a time course of reprogramming (Tran et al., 2019). Using these data, we then chose genes that were expressed in the entire population of

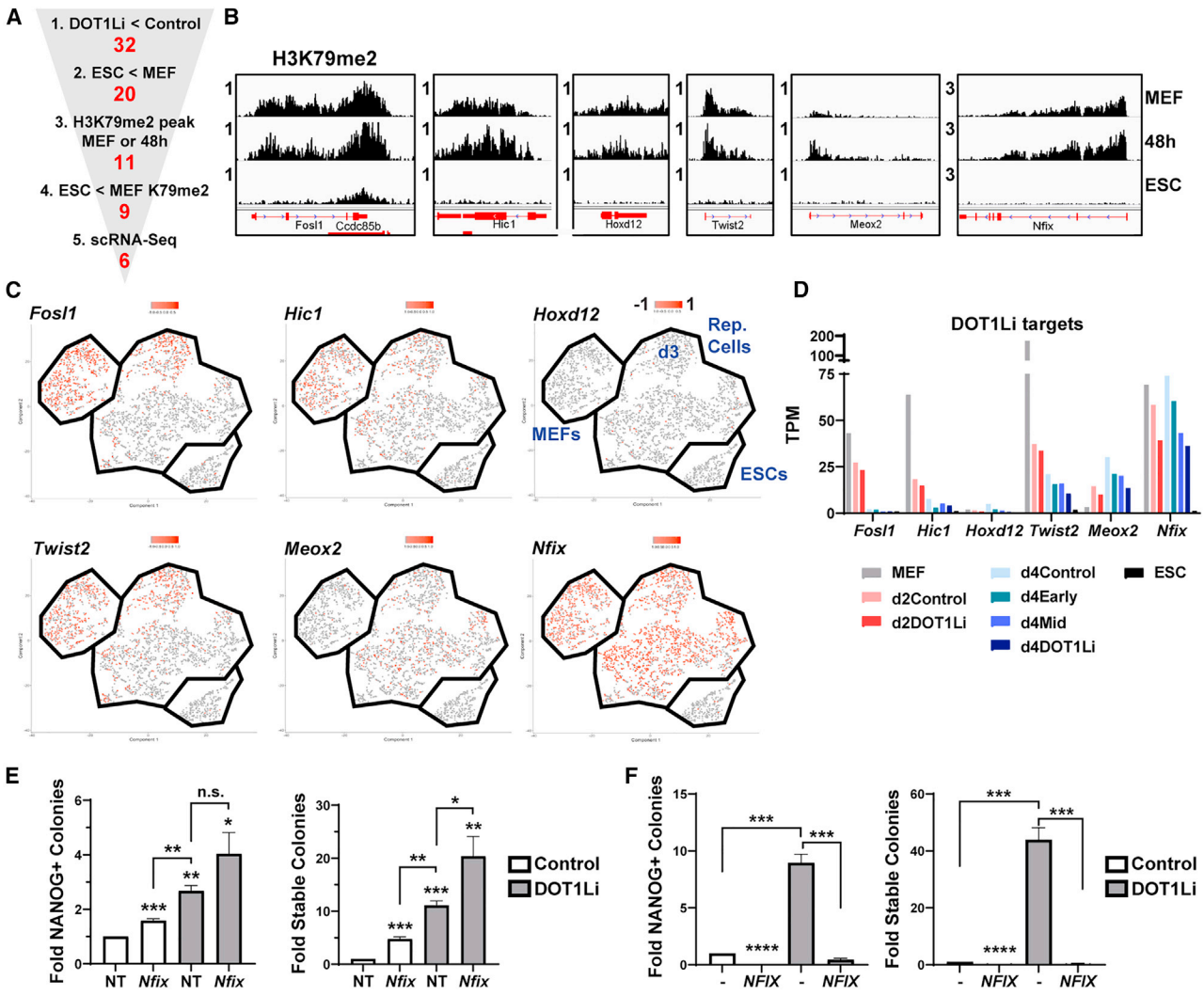

Figure 5. Inhibition of DOT1L enhances reprogramming beyond modulation of single genes

(A) Schematic to identify DOT1L direct target genes. Genes were filtered for (1) at least 2-FC downregulation in expression by DOT1Li treatment at any time point, (2) at least 2-FC downregulation in expression in ESC versus MEFs, (3) a significant gene body H3K79me2 peak (p-4) with 3-fold enrichment over input in MEFs or 48 h OSKM (B), (4) a 2-fold reduction in H3K79me2 gene body reads in ESCs, and (5) expression in a substantial portion of MEFs or reprogramming cells by scRNA-seq (C).

(B) Integrative Genomics Viewer (IGV) tracks of H3K79me2 signal in MEFs, 48 h OSKM, and ESCs of potential DOT1L direct targets.

(C) Cells expressing the DOT1L target gene are labeled in red on the scRNA-seq t-distributed stochastic neighbor embedding (t-SNE). MEFs, reprogramming cells (days 3, 6, 9, and 12), and ESCs are indicated and labeled. Day 3 of reprogramming is indicated, but the other days are mixed, as reprogramming becomes more heterogeneous as it proceeds (Tran et al., 2019).

(D) Expression (TPM) bar graph of candidate DOT1Li downregulated genes.

(E) NANOG$^+$ colonies on days 6 to 7 of reprogramming (left) and stable colonies post-dox removal (right) of cells transfected with NT and siRNA against *Nfix*, treated with control (white bars) or DOT1Li (gray bars). Control-treated NT was set to 1. Error bars represent the SEM of three independent experiment replicates, each consisting of two or three technical replicates. ***p < 0.001, **p < 0.01, *p < 0.05, and n.s., p > 0.05, by unpaired t test.

(F) NANOG$^+$ colonies at day 6 of reprogramming (left) and stable colonies post-dox removal (right) of cells transduced with empty vector control (−) or *NFIX*, treated with control (white bars) or DOT1Li (gray bars). Error bars represent the SEM of three independent experiment replicates, each consisting of two or three technical replicates. ****p < 0.0001 and ***p < 0.001 by unpaired t test.

See also Figure S5.

starting MEFs or reprogramming cells (step 5; Figure 5C), narrowing to six potential targets that could be critical for the mechanism of DOT1Li (Figure 5D). Notably, all six targets were also downregulated by siRNA-mediated *Dot1l* depletion (Figure 3C).

Each target was reduced individually using siRNA-mediated knockdown in the presence or absence of DOT1Li. Depletion of *Fosl1* resulted in cell death with three different siRNAs (data not shown) and was not analyzed further. For each of the other five targets, siRNA-mediated depletion was robust and resulted in a similar fold change compared with that obtained by DOT1Li (Figure S5A). When siRNA for each target was combined with DOT1Li, mRNA levels were further reduced (Figure S5A). *Hic1*, *Hoxd12*, and *Twist2* depletion did not enhance reprogramming in the presence or absence of DOT1Li (Figures S5B and S5C). *Meox2* depletion alone or combined with DOT1Li slightly decreased $NANOG^+$ colony formation (Figure S5B) but did not affect *bona fide* colonies that remained after doxycycline withdrawal (Figure S5C). Depletion of *Nfix* alone increased the occurrence of $NANOG^+$ colonies 2-fold compared with a 3-fold increase with DOT1Li (Figure 5E, left). However, *Nfix* depletion did not lead to a robust formation of *bona fide* colonies, as DOT1Li treatment increased transgene-independent colonies 11-fold, whereas only a 4.8-fold increase was observed with *siNfix* (Figure 5E, right). When combined with DOT1Li, *Nfix* depletion enhanced transgene-independent colony formation (Figure 5E, right). Thus, *Nfix* depletion acts in conjunction with DOT1Li to promote reprogramming.

To interrogate whether these genes are barriers of the process, we overexpressed *MEOX2* and *NFIX* individually in MEFs prior to the induction of reprogramming (Figure S5D). Exogenous *MEOX2* expression inhibited reprogramming on its own but did not affect DOT1Li-mediated reprogramming (Figure S5E, left). Surprisingly, *MEOX2* increased stable colony formation in the absence of DOT1Li (Figure S5E, right). These contrary effects of *Meox2* depletion and overexpression on reprogramming may be related to its heterogeneous expression in the reprogramming population (Figure 5C) and the increase in proliferation in MEFs overexpressing *MEOX2* (data not shown). Ectopic expression of *NFIX* during reprogramming reduced DOT1Li-mediated NANOG acquisition below control levels and prevented stable colony formation (Figure 5F), suggesting it is a potent reprogramming barrier independent of DOT1L activity. Thus, the downregulation of *Nfix* acts in an additive manner to increase pluripotency by contributing to the DOT1Li phenotype.

By comparing the results of the depletion experiments (Figures 5E, S5B, and S5C) with the pattern of expression from single-cell analysis (Figure 5C), we find that DOT1L acts in a collaborative manner with *Nfix* that is still expressed at later stages of reprogramming. *Hic1*, *Fosl1*, and *Twist2* are downregulated in most cells by day 3 of reprogramming, and *Meox2* is upregulated in only a portion of reprogramming cells (Figures 5C and 5D). Taken together with the temporal effectiveness of DOT1Li at the mid stages of reprogramming (Figure 1D), DOT1Li sets the stage for enhancing reprogramming efficiency along with the downregulation of persistently expressed genes such as *Nfix*.

DISCUSSION

DOT1L is crucial for mammalian development, yet its role in cell-fate determination is still unknown. Here, we find that DOT1L is a barrier to pluripotency acquisition of MEFs throughout reprogramming but acts most strongly during mid-reprogramming (Figure 1). Stages of reprogramming when starting from MEFs include an early inactivation of the somatic program, an important component of which is the mesenchymal genes (Li et al., 2010; Samavarchi-Tehrani et al., 2010). Inhibition of DOT1L was reported to enhance human fibroblast reprogramming by facilitating MET (Onder et al., 2012). The reverse process, epithelial to mesenchymal transition (EMT), is prevented in other systems, such as renal (Liu et al., 2019) and breast cancer cell lines (Cho et al., 2015), by DOT1Li. We demonstrate that DOT1L control of cell identity extends far beyond epithelial transitions. Although inhibition of DOT1L increases *Cdh1* expression in our mouse reprogramming studies, it also enhances reprogramming of keratinocytes that do not have to undergo MET and MEF reprogramming post-MET (Figure 4). This corroborates our recent discovery that the epithelial and mesenchymal programs are independently regulated in the presence of DOT1Li during reprogramming using scRNA-seq (Tran et al., 2019).

In the course of assessing DOT1L transcriptional regulation, we identified contributions of the reprogramming barrier *Nfix* that maintain cellular identity with DOT1L (Figure 5). NFIX is a transcription factor important for neural (Pekarik and Belmonte, 2008) and muscle development (Pistocchi et al., 2013). In addition, NFIX is required to maintain murine hair follicle stem cell enhancer function (Adam et al., 2020), and its depletion increases the number of pluripotent colonies (Yang et al., 2011). From our previous analysis of reprogramming with scRNA-seq, we ordered single cells in a trajectory (Tran et al., 2019). We found a major branchpoint where cells stalled and did not complete the transition to iPSCs (Tran et al., 2019). *Nfix* was found to be a branchpoint gene such that downregulation was required to continue in the reprogramming trajectory, further suggesting that it may have a specific role in mid-

reprogramming. Of the identified DOT1L targets, *Nfix* continues to be expressed in cells later in reprogramming and gains H3K79me2 after OSKM induction (Figures 5B and 5C), suggesting DOT1Li may facilitate its downregulation by preventing the gain in H3K79me2 enrichment at later reprogramming time points. This result is in contrast to previous findings that DOT1Li enhances pluripotency acquisition by downregulation of the established transcriptional program (Onder et al., 2012). It is important to note that depletion of *Nfix* does not reach the reprogramming efficiency of DOT1Li, and the effect is additive with DOT1Li (Figure 5E). Thus, downregulation of reprogramming-associated factors may contribute but is not solely causal of the DOT1L reprogramming phenotype.

We find that modulation of DOT1L-DE genes does not substitute for DOT1L catalytic inhibition (Figures 4 and 5), suggesting that H3K79me may have a role in reprogramming beyond transcriptional regulation of single genes. During development, only four genes were DE in *Dot1l* KO mouse c-kit^{+} cells sorted from embryonic day 10.5 (E10.5) yolk sacs, where profound phenotypic alterations in vascular morphology and erythrocyte maturation were observed (Feng et al., 2010). These small transcriptional changes in key factors like *Nanog* during reprogramming or *Gata2* during erythrocyte maturation suggest that loss of H3K79me may alter global epigenetic profiles rather than local expression profiles. For example, loss of H3K79me2 allowed for spread of H3K27me3 on downregulated genes in leukemia cells (Deshpande et al., 2014). H3K79me2/3 are enriched at certain intronic enhancers in leukemia cell lines and regulate future deposition of H3K27ac (Godfrey et al., 2019), a modification associated with enhancer activity. In neural differentiation, DOT1Li decreased accessibility of a subset of enhancers (Ferrari et al., 2020). In support of further epigenetic alterations, both upregulated and downregulated genes can be decorated by H3K79me2 before DOT1L depletion in development of the cerebral cortex (Franz et al., 2019). Thus, H3K79me may affect histone modification, depending on chromatin context.

We observed that many more genes are upregulated rather than downregulated in their steady-state expression by DOT1Li during reprogramming (Figures 1 and 4). Many of the upregulated genes are expressed in other lineages and are not modified by H3K79me2 in MEFs or ESCs (Figures 3 and S3D). Alternatively, these genes may be regulated indirectly by the binding of DOT1Li-DE transcription factors, such as HOXD12 or HIC1. The aberrant expression of lineage-specific genes may promote reprogramming, a notion that can be further investigated by single-cell transcriptional analysis. Regardless, the boost to reprogramming cells by DOT1Li seems to outweigh the burden of spurious lineage gene expression. Taken together, our results demonstrate that DOT1L activity functions beyond steady-state alterations to the somatic transcriptome; rather it collaborates with reprogramming-associated factors to safeguard cell identity.

EXPERIMENTAL PROCEDURES

Cell isolation and culture

Male and female MEFs were isolated on E13.5 from embryos that were homozygous for the *Oct4*-2A-*Klf4*-2A-IRES-*Sox2*-2A-*c-Myc* (OKSM) transgene at the *Col1a1* locus and either heterozygous or homozygous for the reverse tetracycline transactivator (rtTA) allele at the *Rosa26* locus, as previously described (Tran et al., 2019). MEFs were grown in DMEM, 10% fetal bovine serum (FBS), 1× non-essential amino acids, 1× GlutaMAX, 1× penicillin/streptomycin, and 2-mercaptoethanol (4 μL/500 mL). Feeder MEFs were maintained and isolated as above from DR4 mice genetically resistant to geneticin (G418), puromycin, hygromycin, and 6-thioguanine. Feeder cells were irradiated with 9,000 rad after three passages. ESCs V6.5 were grown on feeder MEFs in KO DMEM, 15% FBS, 1× non-essential amino acids, 1× GlutaMAX, 1× penicillin/streptomycin, 2-mercaptoethanol (4 μL/525 mL), and leukemia inhibitory factor. Keratinocytes were isolated from reprogrammable mice 4 days postnatal as previously described (Li et al., 2017) and cultured in EpiLife medium with 60 μM calcium (Thermo Fisher Scientific MEPI500CA) with the EpiLife defined growth supplement (Thermo Fisher Scientific S0125). 293T cells were acquired from ATCC and grown in DMEM and 10% FBS. Mice were maintained according to the UW-Madison institutional animal care and use committee (IACUC)-approved protocol.

A detailed description of all materials and methods is provided in the supplemental information.

Data and code availability

The accession number for all RNA-seq datasets reported in this paper is National Center for Biotechnology Information Gene Expression Omnibus (GEO): GSE160580.

SUPPLEMENTAL INFORMATION

Supplemental information can be found online at https://doi.org/10.1016/j.stemcr.2021.12.004.

AUTHOR CONTRIBUTIONS

C.K.W. performed experiments and bioinformatic analysis, C.K.W. and R.S. wrote the manuscript and acquired funding, and R.S. conceived and directed the project.

CONFLICT OF INTERESTS

The authors declare no competing interests.

ACKNOWLEDGMENTS

This work was supported by a UW-Madison Stem Cell and Regenerative Medicine Center postdoctoral award to C.K.W., a UW-Madison Fall competition, and a Shaw Scientist award to the R.S. lab. We thank Dr. Roice Wille for R script design, Stefan Pietrzak and

Brenton Halvorson for scRNA-seq analysis, Dr. Jason Tchieu for the *NFIX* vector, and Dr. Konstantinos Chronis and the R.S. lab members for critical reading of the manuscript.

Received: December 24, 2020
Revised: December 6, 2021
Accepted: December 7, 2021
Published: January 6, 2022

REFERENCES

Adam, R.C., Yang, H., Ge, Y., Infarinato, N.R., Gur-Cohen, S., Miao, Y., Wang, P., Zhao, Y., Lu, C.P., Kim, J.E., et al. (2020). NFI transcription factors provide chromatin access to maintain stem cell identity while preventing unintended lineage fate choices. Nat. Cell Biol. *22*, 640–650.

Apostolou, E., and Hochedlinger, K. (2013). Chromatin dynamics during cellular reprogramming. Nature *502*, 462–471.

Barry, E.R., Krueger, W., Jakuba, C.M., Veilleux, E., Ambrosi, D.J., Nelson, C.E., and Rasmussen, T.P. (2009). ES cell cycle progression and differentiation require the action of the histone methyltransferase Dot1L. Stem Cells *27*, 1538–1547.

Black, J.C., Van Rechem, C., and Whetstine, J.R. (2012). Histone lysine methylation dynamics: establishment, regulation, and biological impact. Mol. Cell *48*, 491–507.

Borkent, M., Bennett, B.D., Lackford, B., Bar-Nur, O., Brumbaugh, J., Wang, L., Du, Y., Fargo, D.C., Apostolou, E., Cheloufi, S., et al. (2016). A serial shRNA screen for roadblocks to reprogramming identifies the protein modifier SUMO2. Stem Cell Rep. *6*, 704–716.

Campbell, C.T., Haladyna, J.N., Drubin, D.A., Thomson, T.M., Maria, M.J., Yamauchi, T., Waters, N.J., Olhava, E.J., Pollock, R.M., Smith, J.J., et al. (2017). Mechanisms of Pinometostat (EPZ-5676) treatment-emergent resistance in MLL-rearranged leukemia. Mol. Cancer Ther. *16*, 1669–1679.

Cao, K., Ugarenko, M., Ozark, P.A., Wang, J., Marshall, S.A., Rendleman, E.J., Liang, K., Wang, L., Zou, L., Smith, E.R., et al. (2020). DOT1L-controlled cell-fate determination and transcription elongation are independent of H3K79 methylation. Proc. Natl. Acad. Sci. U S A *117*, 27365–27373.

Castaño Betancourt, M.C., Cailotto, F., Kerkhof, H.J., Cornelis, F.M.F., Doherty, S.A., Hart, D.J., Hofman, A., Luyten, F.P., Maciewicz, R.A., Mangino, M., et al. (2012). Genome-wide association and functional studies identify the DOT1L gene to be involved in cartilage thickness and hip osteoarthritis. Proc. Natl. Acad. Sci. U S A. *109*, 8218–8223.

Chen, T., Yuan, D., Wei, B., Jiang, J., Kang, J., Ling, K., Gu, Y., Li, J., Xiao, L., and Pei, G. (2010). E-cadherin-mediated cell-cell contact is critical for induced pluripotent stem cell generation. Stem Cells *28*, 1315–1325.

Cho, M.-H., Park, J.-H., Choi, H.-J., Park, M.-K., Won, H.-Y., Park, Y.-J., Lee, C.H., Oh, S.-H., Song, Y.-S., Kim, H.S., et al. (2015). DOT1L cooperates with the c-Myc-p300 complex to epigenetically derepress CDH1 transcription factors in breast cancer progression. Nat. Commun. *6*, 7821.

Chronis, C., Fiziev, P., Papp, B., Butz, S., Bonora, G., Sabri, S., Ernst, J., and Plath, K. (2017). Cooperative binding of transcription factors orchestrates reprogramming. Cell *168*, 442–459.e20.

Daigle, S.R., Olhava, E.J., Therkelsen, C.A., Basavapathruni, A., Jin, L., Boriack-Sjodin, P.A., Allain, C.J., Klaus, C.R., Raimondi, A., Scott, M.P., et al. (2013). Potent inhibition of DOT1L as treatment of MLL-fusion leukemia. Blood *122*, 1017–1025.

Dang-Nguyen, T.Q., and Torres-Padilla, M.-E. (2015). How cells build totipotency and pluripotency: nuclear, chromatin and transcriptional architecture. Curr. Opin. Cell Biol. *34*, 9–15.

Deshpande, A.J., Deshpande, A., Sinha, A.U., Chen, L., Chang, J., Cihan, A., Fazio, M., Chen, C., Zhu, N., Koche, R., et al. (2014). AF10 regulates progressive H3K79 methylation and HOX gene expression in diverse AML subtypes. Cancer Cell *26*, 896–908.

Duffy, E.E., Canzio, D., Maniatis, T., and Simon, M.D. (2018). Solid phase chemistry to covalently and reversibly capture thiolated RNA. Nucleic Acids Res. *46*, 6996–7005.

Feng, Y., Yang, Y., Ortega, M.M., Copeland, J.N., Zhang, M., Jacob, J.B., Fields, T.A., Vivian, J.L., and Fields, P.E. (2010). Early mammalian erythropoiesis requires the Dot1L methyltransferase. Blood *116*, 4483–4491.

Ferrari, F., Arrigoni, L., Franz, H., Izzo, A., Butenko, L., Trompouki, E., Vogel, T., and Manke, T. (2020). DOT1L-mediated murine neuronal differentiation associates with H3K79me2 accumulation and preserves SOX2-enhancer accessibility. Nat. Commun. *11*, 5200.

Franz, H., Villarreal, A., Heidrich, S., Videm, P., Kilpert, F., Mestres, I., Calegari, F., Backofen, R., Manke, T., and Vogel, T. (2019). DOT1L promotes progenitor proliferation and primes neuronal layer identity in the developing cerebral cortex. Nucleic Acids Res. *47*, 168–183.

Godfrey, L., Crump, N.T., Thorne, R., Lau, I.-J., Repapi, E., Dimou, D., Smith, A.L., Harman, J.R., Telenius, J.M., Oudelaar, A.M., et al. (2019). DOT1L inhibition reveals a distinct subset of enhancers dependent on H3K79 methylation. Nat. Commun. *10*, 2803.

Hawkins, K., Mohamet, L., Ritson, S., Merry, C.L.R., and Ward, C.M. (2012). E-cadherin and, in its absence, N-cadherin promotes Nanog expression in mouse embryonic stem cells via STAT3 phosphorylation. Stem Cells *30*, 1842–1851.

Jackson, S.A., Olufs, Z.P.G., Tran, K.A., Zaidan, N.Z., and Sridharan, R. (2016). Alternative routes to induced pluripotent stem cells revealed by reprogramming of the neural lineage. Stem Cell Rep. *6*, 302–311.

Jones, B., Su, H., Bhat, A., Lei, H., Bajko, J., Hevi, S., Baltus, G.A., Kadam, S., Zhai, H., Valdez, R., et al. (2008). The histone H3K79 methyltransferase Dot1L is essential for mammalian development and heterochromatin structure. Plos Genet. *4*, e1000190.

Kaniskan, H.Ü., Martini, M.L., and Jin, J. (2018). Inhibitors of protein methyltransferases and demethylases. Chem. Rev. *118*, 989–1068.

Kelsey, G., Stegle, O., and Reik, W. (2017). Single-cell epigenomics: recording the past and predicting the future. Science *358*, 69–75.

Kwesi-Maliepaard, E.M., Aslam, M.A., Alemdehy, M.F., van den Brand, T., McLean, C., Vlaming, H., van Welsem, T., Korthout, T., Lancini, C., Hendriks, S., et al. (2020). The histone

methyltransferase DOT1L prevents antigen-independent differentiation and safeguards epigenetic identity of CD8+ T cells. Proc. Natl. Acad. Sci. U S A. *117*, 20706–20716.

Li, F., Adase, C.A., and Zhang, L.-J. (2017). Isolation and culture of primary mouse keratinocytes from neonatal and adult mouse skin. J. Vis. Exp. *125*, e56027.

Li, R., Liang, J., Ni, S., Zhou, T., Qing, X., Li, H., He, W., Chen, J., Li, F., Zhuang, Q., et al. (2010). A mesenchymal-to-epithelial transition initiates and is required for the nuclear reprogramming of mouse fibroblasts. Cell Stem Cell *7*, 51–63.

Liu, L., Zou, J., Guan, Y., Zhang, Y., Zhang, W., Zhou, X., Xiong, C., Tolbert, E., Zhao, T.C., Bayliss, G., et al. (2019). Blocking the histone lysine 79 methyltransferase DOT1L alleviates renal fibrosis through inhibition of renal fibroblast activation and epithelial-mesenchymal transition. FASEB J. *33*, 11941–11958.

Mohan, M., Lin, C., Guest, E., and Shilatifard, A. (2010). Licensed to elongate: a molecular mechanism for MLL-based leukaemogenesis. Nat. Rev. Cancer *10*, 721–728.

Nassa, G., Salvati, A., Tarallo, R., Gigantino, V., Alexandrova, E., Memoli, D., Sellitto, A., Rizzo, F., Malanga, D., Mirante, T., et al. (2019). Inhibition of histone methyltransferase DOT1L silences ERα gene and blocks proliferation of antiestrogen-resistant breast cancer cells. Sci. Adv. *5*, eaav5590.

Nefzger, C.M., Rossello, F.J., Chen, J., Liu, X., Knaupp, A.S., Firas, J., Paynter, J.M., Pflueger, J., Buckberry, S., Lim, S.M., et al. (2017). Cell type of origin dictates the route to pluripotency. Cell Rep *21*, 2649–2660.

Nguyen, A.T., and Zhang, Y. (2011). The diverse functions of Dot1 and H3K79 methylation. Genes Dev. *25*, 1345–1358.

Onder, T.T., Kara, N., Cherry, A., Sinha, A.U., Zhu, N., Bernt, K.M., Cahan, P., Marcarci, B.O., Unternaehrer, J., Gupta, P.B., et al. (2012). Chromatin-modifying enzymes as modulators of reprogramming. Nature *483*, 598–602.

Ooga, M., Inoue, A., Kageyama, S., Akiyama, T., Nagata, M., and Aoki, F. (2008). Changes in H3K79 methylation during preimplantation development in mice. Biol. Reprod. *78*, 413–424.

Pekarik, V., and Belmonte, J.C.I. (2008). NFIX–one gene, two knockouts, multiple effects. J. Biol. *7*, 29.

Pistocchi, A., Gaudenzi, G., Foglia, E., Monteverde, S., Moreno-Fortuny, A., Pianca, A., Cossu, G., Cotelli, F., and Messina, G. (2013). Conserved and divergent functions of Nfix in skeletal muscle development during vertebrate evolution. Development *140*, 1528–1536.

Polo, J.M., Anderssen, E., Walsh, R.M., Schwarz, B.A., Nefzger, C.M., Lim, S.M., Borkent, M., Apostolou, E., Alaei, S., Cloutier, J., et al. (2012). A molecular roadmap of reprogramming somatic cells into iPS cells. Cell *151*, 1617–1632.

Samavarchi-Tehrani, P., Golipour, A., David, L., Sung, H.-K., Beyer, T.A., Datti, A., Woltjen, K., Nagy, A., and Wrana, J.L. (2010). Functional genomics reveals a BMP-driven mesenchymal-to-epithelial transition in the initiation of somatic cell reprogramming. Cell Stem Cell *7*, 64–77.

Smith, Z.D., and Meissner, A. (2013). DNA methylation: roles in mammalian development. Nat. Rev. Genet. *14*, 204–220.

Sridharan, R., Gonzales-Cope, M., Chronis, C., Bonora, G., McKee, R., Huang, C., Patel, S., Lopez, D., Mishra, N., Pellegrini, M., et al. (2013). Proteomic and genomic approaches reveal critical functions of H3K9 methylation and heterochromatin protein-1γ in reprogramming to pluripotency. Nat. Cell Biol. *15*, 872–882.

Tran, K.A., Pietrzak, S.J., Zaidan, N.Z., Siahpirani, A.F., McCalla, S.G., Zhou, A.S., Iyer, G., Roy, S., and Sridharan, R. (2019). Defining reprogramming checkpoints from single-cell analyses of induced pluripotency. Cell Rep. *27*, 1726–1741.e5.

Veloso, A., Kirkconnell, K.S., Magnuson, B., Biewen, B., Paulsen, M.T., Wilson, T.E., and Ljungman, M. (2014). Rate of elongation by RNA polymerase II is associated with specific gene features and epigenetic modifications. Genome Res. *24*, 896–905.

Wu, A., Zhi, J., Tian, T., Cihan, A., Cevher, M.A., Liu, Z., David, Y., Muir, T.W., Roeder, R.G., and Yu, M. (2021). DOT1L complex regulates transcriptional initiation in human erythroleukemic cells. Proc. Natl. Acad. Sci. U S A *118*, e2106148118.

Yang, C.-S., Lopez, C.G., and Rana, T.M. (2011). Discovery of nonsteroidal anti-inflammatory drug and anticancer drug enhancing reprogramming and induced pluripotent stem cell generation. Stem Cells *29*, 1528–1536.

Yu, W., Chory, E.J., Wernimont, A.K., Tempel, W., Scopton, A., Federation, A., Marineau, J.J., Qi, J., Barsyte-Lovejoy, D., Yi, J., et al. (2012). Catalytic site remodelling of the DOT1L methyltransferase by selective inhibitors. Nat. Commun. *3*, 1288.

Zhang, W., Xia, X., Reisenauer, M.R., Hemenway, C.S., and Kone, B.C. (2006). Dot1a-AF9 complex mediates histone H3 Lys-79 hypermethylation and repression of ENaCα in an aldosterone-sensitive manner. J. Biol. Chem. *281*, 18059–18068.

Stem Cell Reports, Volume *17*

Supplemental Information

DOT1L inhibition enhances pluripotency beyond acquisition of epithelial identity and without immediate suppression of the somatic transcriptome

Coral K. Wille and Rupa Sridharan

Figure S1 related to Figure 1

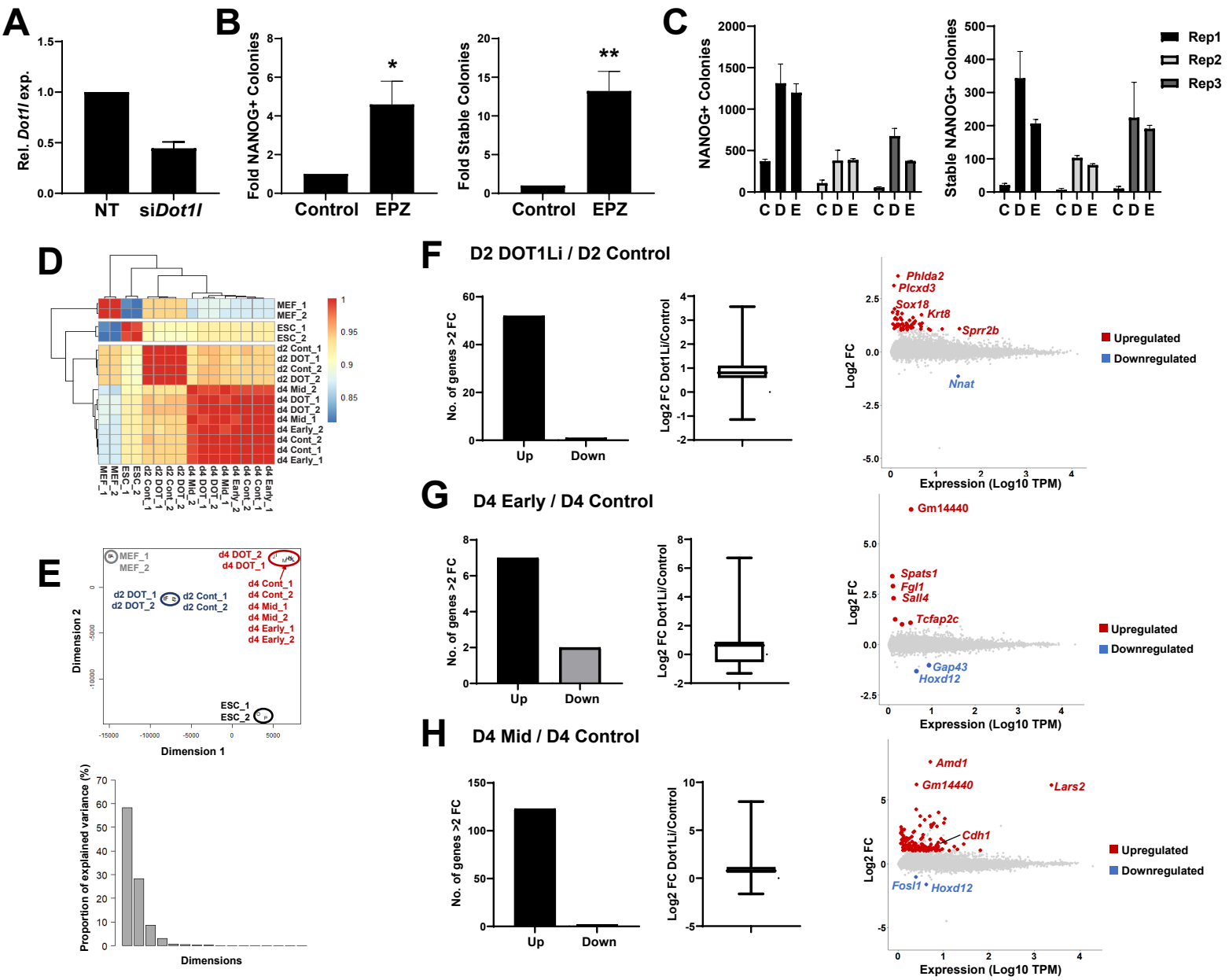

Figure S1. Loss of H3K79me during reprogramming results in few steady-state transcriptional changes.

A. Relative *Dot1l* expression measured on day 2 of reprogramming. Nontargeting (NT) siRNA treated cells set to 1.

B. Reprogramming efficiency (Left) and stable NANOG+ colonies post dox withdrawal (Right) of MEFs treated with control and EPZ5676 (EPZ). Colonies obtained in control treatment set to 1. Error bars represent the SEM of three independent experiment replicates, each comprised of 2 technical replicates. **P<0.01 and *P<0.05 by unpaired t-test.

C. Average colonies obtained (Left) and stable NANOG+ colonies post dox withdrawal (Right) in each independent experiment replicate (Rep), of MEFs treated with control (C), DOT1Li (D), and EZP5676 (E). Error bars represent the SEM of 2 technical replicates.

D. Pearson correlation of all timecourse RNA-Seq independent experiment replicates. Notations: Day (d), control treatment (Cont), and DOT1Li (DOT).

E. Top: PCA of all timecourse RNA-Seq independent experiment replicates. MEFs notated in gray, reprogramming day 2 in blue, reprogramming day 4 in red, and ESCs in black. Bottom: Percent of variance explained by each component.

F-H. Left: Number of genes upregulated or downregulated more than 2-fold change (FC) with a posterior probability of differential expression greater than 0.95 determined by EBSeq. Middle: Box plot of Log2 FC of all genes with a posterior probability of differential expression greater than 0.95. Right: Expression measured as Log10 of the averaged transcripts per million (TPM) of the two samples versus Log2 FC of all genes. More than 2-fold upregulated indicated in red and downregulated indicated in blue. F. Day 2 DOT1Li versus day 2 Control, G. Day 4 Early (days 0-2) DOT1Li versus day 4 Control, H. Day 4 Mid (days 2-4) DOT1Li versus day 4 Control.

Figure S2 related to Figure 2

A

GO Term	Significance	Number	Examples
Cellular macromolecule metabolic process	6.4E-91	3900	*Arl2bp*, *Ddx49*
Nucleic acid metabolic process	4.5E-73	2605	*Polr2e*, *Ets1*
RNA binding	1.8E-62	581	*Oas1h*, *Esf1*
Gene expression	2.5E-57	1315	*Eif4a1*, *Med10*

B

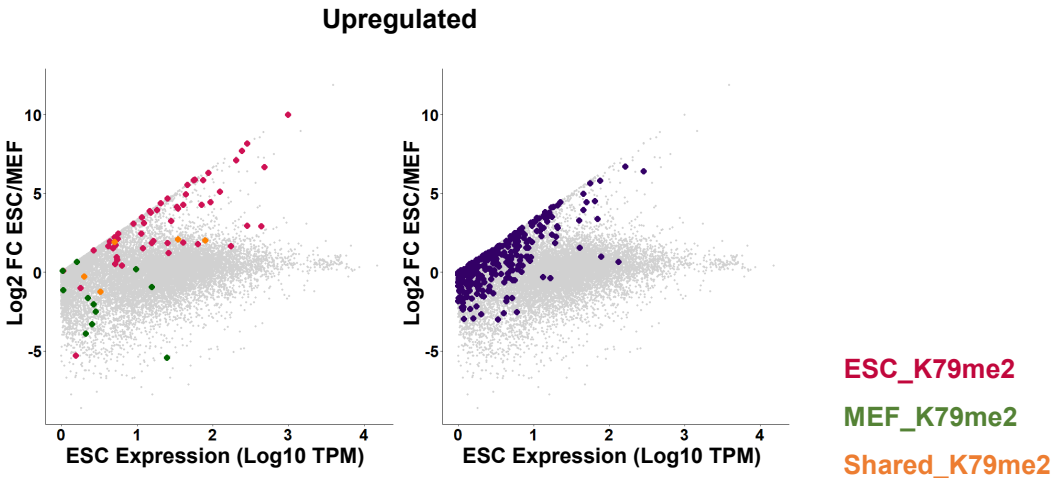

C

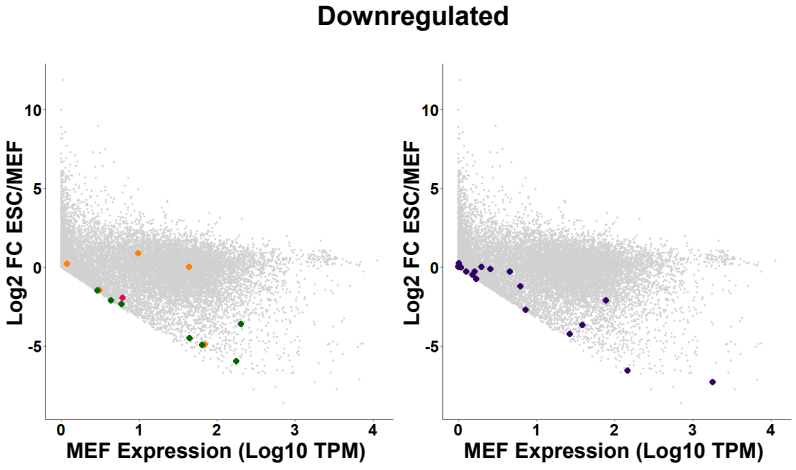

Figure S2. H3K79me2 is enriched on numerous genes yet few change transcriptionally in steady state mRNA levels.

A. Most significant gene ontology (GO) terms of genes that have an H3K79me2 peak shared in both MEFs and ESCs (Fig 2B, orange).

B. H3K79me2 peak status of DOT1Li upregulated genes designated by color, plotted on ESC expression measured as Log10 TPM versus Log2 fold change (FC) in ESCs relative to MEFs of all genes.

C. H3K79me2 peak status of DOT1Li downregulated genes designated by color, plotted on MEF expression measured as Log10 TPM versus Log2 fold change (FC) in ESCs relative to MEFs of all genes.

Figure S3 related to Figure 3

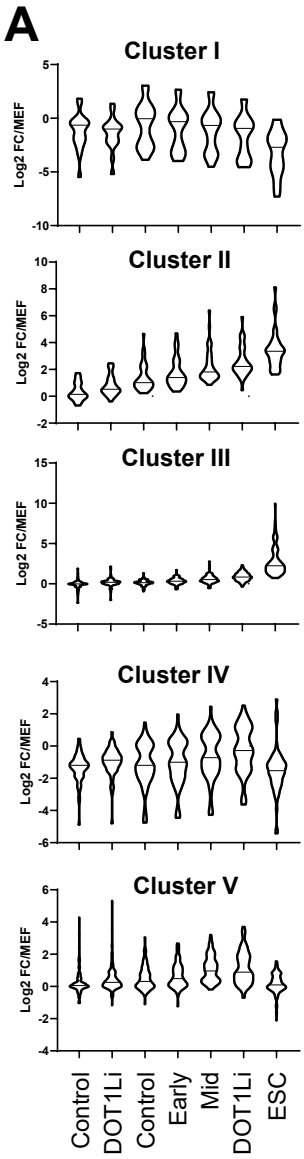

B

Motif	Cluster	p-value	Percent of targets	Function
E-Box (SNAI2) (ZEB1)	II III	1E-02 1E-10	50.0% 39.8%	Repressor
TCF7	IV	1E-7	16.7%	Activator
HOXD12	V	1E-05	2.1%	Activator
HIC1	II/III V	1E-05 1E-02	4.0% 77.8%	Repressor

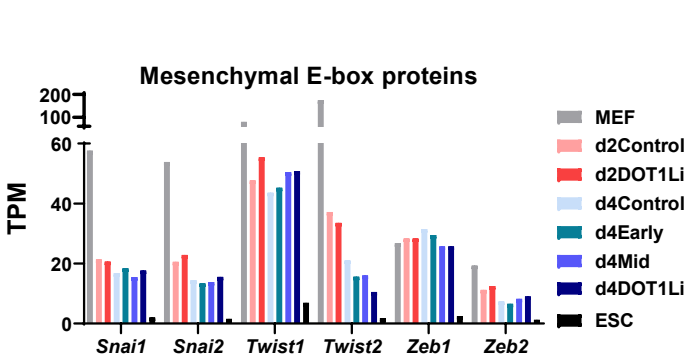

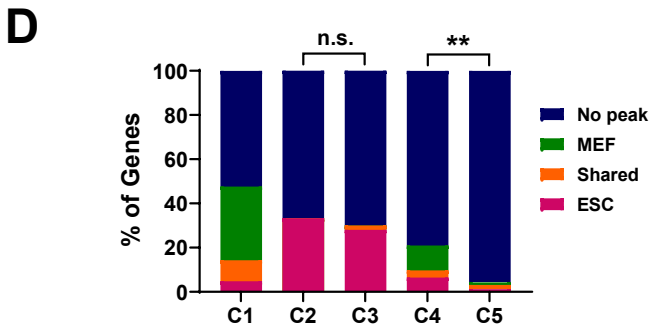

Figure S3. DOT1L inhibition leads to transcriptional changes not observed in MEFs or ESCs.

A. Violin plot of Log2 fold change (FC) TPM relative to MEFs for each cluster.

B. Table of motifs in each cluster identified with HOMER. The p-value, percent of targets within the cluster, and function of the binding protein for motifs bound by DOT1Li-DE genes are displayed.

C. Expression (TPM) bar graph of mesenchymal E-box binding proteins.

D. Bar graph of the percentage of genes with an H3K79me2 called peak in each cluster. Significance determined by Fisher's exact test. All pairwise comparison are ****P<0.0001, except those noted as **P<0.01 or not significant (n.s.) P>0.05.

Figure S4 related to Figure 4

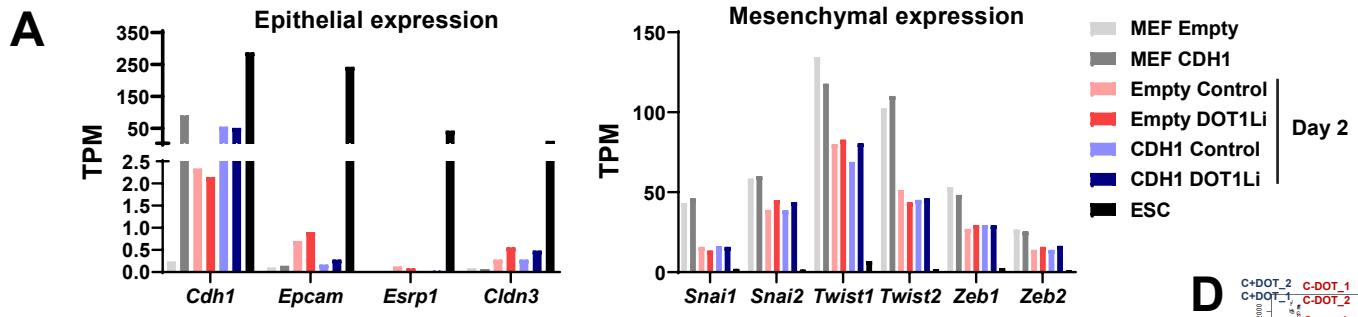

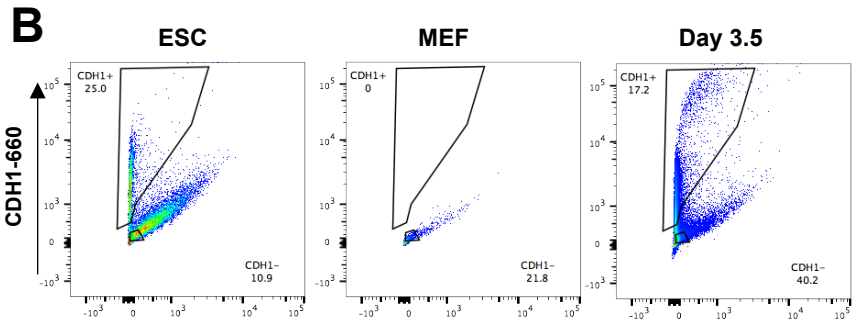

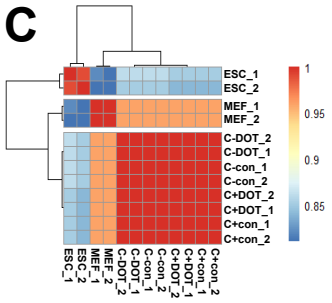

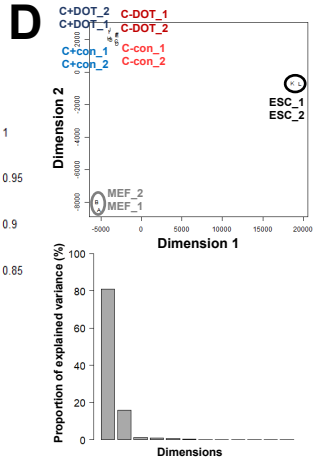

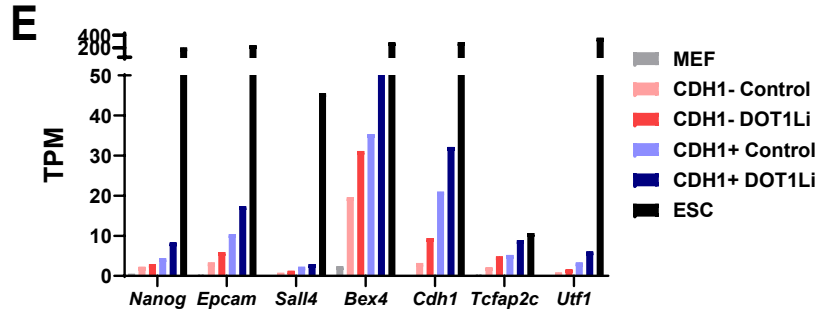

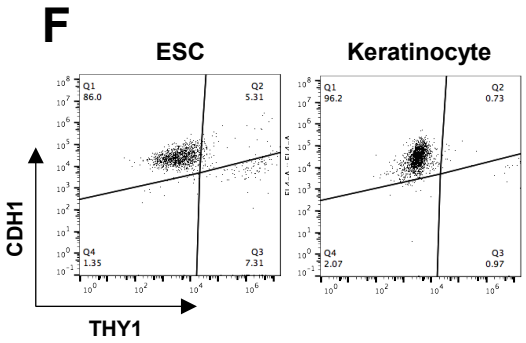

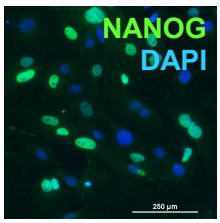

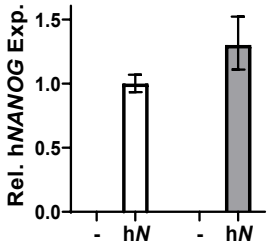

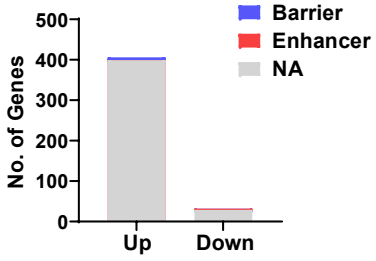

Borkent et al., Stem Cell Reports, 2016

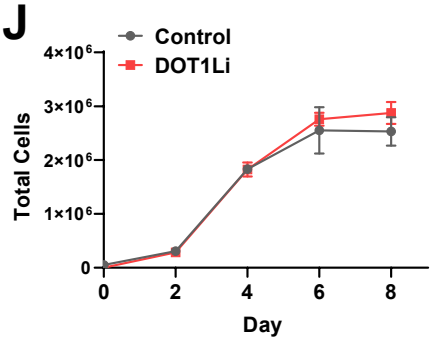

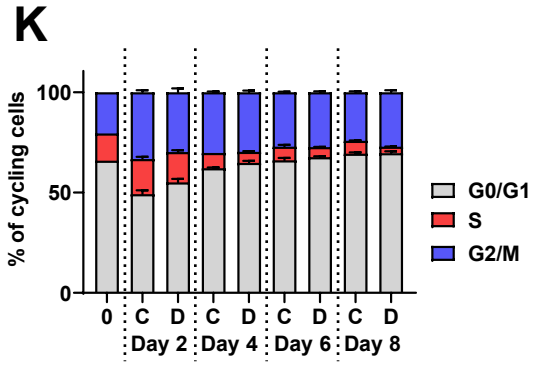

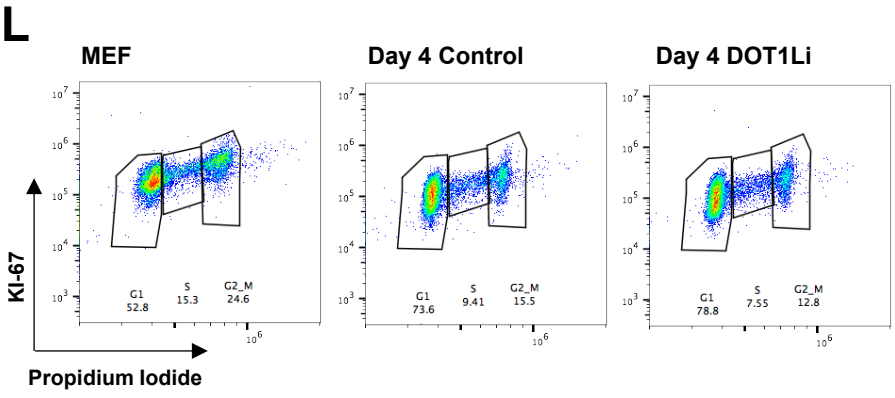

Figure S4. Inhibition of DOT1L enhances reprogramming of epithelial cells.

A. Expression (TPM) bar graphs of MEFs and day 2 reprogramming cells transduced with empty vector control or *Cdh1*, treated with and without DOT1Li.

B. Flow cytometry sorting of CDH1 positive and negative cells for Fig 4C with ESC and MEF controls. Gates indicate collected cells.

C. Pearson correlation of all CDH1 sort RNA-Seq independent experiment replicates. Notations: CDH1- (C-), CDH1+ (C+), control treatment (con), and DOT1Li (DOT).

D. Top: PCA of all CDH1 sort RNA-Seq independent experiment replicates. MEFs notated in gray, CDH1- (C-) reprogramming in red, CDH1+ (C+) reprogramming in blue, and ESCs in black. Bottom: Percent of variance explained by each component.

E. Expression (TPM) bar graph of representative upregulated genes in CDH1- and CDH1+ that overlapped with genes upregulated in ESCs relative to MEFs (Fig 4E).

F. Flow cytometry analysis of THY1 and CDH1 on ESCs and keratinocytes.

G. Immunofluorescence of human NANOG transduced in MEFs. Scale bar = 250 μM.

H. Relative human *NANOG* expression measured on day 4 of reprogramming in cells treated with control (white bars) or DOT1Li (gray bars). Control treated cells transduced with h*NANOG* set to one.

I. Overlap of DOT1Li-DE genes and Borket et al., 2016 screen. Genes chosen for overlap affected reprogramming more than 2-fold. “Barriers” indicate genes targeted by shRNAs enriched in reprogrammed cells and “enhancers” are genes targeted by shRNAs depleted in reprogrammed cells.

J. Cells treated with control (gray) or DOT1Li (red) were counted every two days during reprogramming. Error bars represent the SD of three technical replicates.

K. Quantification of cell cycle analysis. Cells on day 0 (0), and cells treated with DOT1Li (D) or control (C) were assessed every two days during reprogramming.

L. Representative propidium iodide and KI-67 flow cytometry cell cycle analysis (Fig S4K).

Figure S5 related to Figure 5

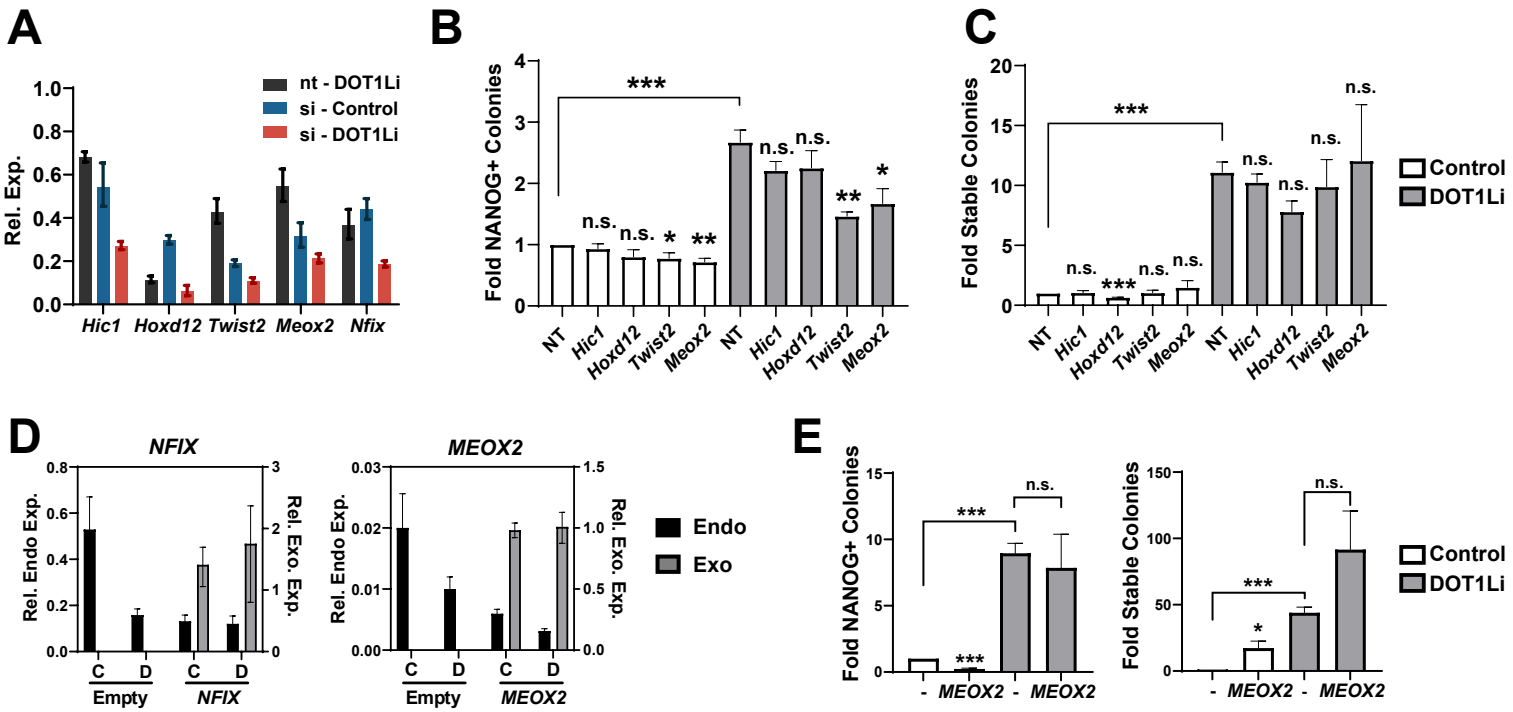

Figure S5. Inhibition of DOT1L enhances reprogramming beyond modulation of single genes.

A. Relative expression of si-depleted genes on day 4 of reprogramming. Cells transduced with nontargeting (NT) siRNA treated with control set to 1.

B. NANOG+ colonies on days 6-7 of reprogramming of cells transfected with nontargeting (NT) and siRNA against the indicated DOT1L direct target gene, treated with control (white bars) or DOT1Li (gray bars). Control treated NT set to 1. Error bars represent the SEM of 3-4 independent experiment replicates, each consisting of 2-3 technical replicates. ***P<0.001, **P<0.01, *P<0.05, and not significant (n.s.) P>0.05 by unpaired t test.

C. Transgene independent stable colonies post dox removal of cells transfected with nontargeting (NT) and siRNA against the indicated DOT1L direct target gene, treated with control (white bars) or DOT1Li (gray bars). Control treated NT set to 1. Error bars represent the SEM of 3-4 independent experiment replicates, each consisting of 2-3 technical replicates. ***P<0.001 and not significant (n.s.) P>0.05 by unpaired t test.

D. Relative expression of endogenous (Endo) in black and exogenous (Exo) in gray of *NFIX* (Left) and *MEOX2* (Right) on day 4 of reprogramming. Cells were treated with Control (C) or DOT1Li (D).

E. NANOG+ colonies at day 6 of reprogramming (Left) and stable colonies post dox removal (Right) of cells transduced with empty vector control (-) or *MEOX2*, treated with control (white bars) or DOT1Li (gray bars). Error bars represent the SEM of 3 independent experiment replicates, each consisting of 2-3 technical replicates. ***P<0.001, *P<0.05, and not significant (n.s.) P>0.05 by unpaired t test.

SUPPLEMENTAL EXPERIMENTAL PROCEDURES

Reprogramming experiments

MEFs were seeded at a density of 30,000 to 50,000 cells/12-well or 20,000 cells/24-well onto gelatinized coverslips. Keratinocytes were seeded at a density of 10,000 cells/24 well onto gelatinized coverslips. Feeder MEFs were added at 1/2x confluency and reprogramming was initiated with 2 µg/ml of doxycycline (dox) with either vehicle (DMSO) control, 5 µM SGC0946/DOT1Li (ApexBio A4167), or 3 µM EPZ5676 (MedChem Express HY-15593). ESC media made with FBS or knock-out serum replacement (KSR), as indicated, with fresh dox and chemicals was replaced every two days. Keratinocytes were maintained in keratinocyte media two days post-OSKM induction before changing to ESC media to avoid FBS-induced differentiation. In the case of exogenous gene expression, MEFs were transduced with lentivirus and selected (if possible) before seeding.

To assess transgene independence, reprogramming cells were washed once with ESC media, and ESC media free of doxycycline and drugs was replaced in wells. Sustained NANOG expression was measured 2-4 days post doxycycline removal by immunofluorescence. Experiments were timed for individual MEFs so that cells were exposed sufficiently to OSKM to produce *bona fide* colonies, but not so long that NANOG positive colonies were overcrowded and uncountable in the presence of doxycycline.

Reprogramming statistical analysis

A colony was considered a grouping of 4 or more NANOG+ cells. Each independent experiment replicate was derived from an independent MEF isolation, and was the average of 2-3 technical replicates. Technical replicates consisted of coverslips in individual wells of a single experimental replicate. Fold was calculated relative to the control condition unless otherwise indicated, and error bars depict the standard error of the mean (SEM) of independent experiment replicates. Experimental replicate (n) information is listed in each figure legend. Significance was calculated as specified in legends using Graphpad Prism 9 for figures aggregated from three or more independent experiment replicates. To compare two conditions, significance was calculated using the unpaired two-tailed t-test function. Comparison among 3 samples was performed with one-way ANOVA repeated measure, matched based independent experiment replicate. The mean of every sample group was compared post-hoc using the Tukey test to calculate significance for multiple comparisons.

Lentiviral vectors, packaging, and transduction

NANOG (Addgene 16578), *MEOX2* (Addgene 116761), and *Cdh1* (Addgene 71366) were acquired from Addgene. The CDS of *Cdh1* was amplified from Addgene 71366 with 5'-TGTTTCGAAATGGGAGCCCGGTGCCGC-3' and 5'-TGTGCGGCCGCTTAGTCGTCCTCGCCACCGCC-3', and moved into the BstBI and NotI sites of pCDH-CMV-MCS-EF1α-Neo. The CDS of human *NFIX* (NM_002501.4) was cloned in to the EcoRI site of Tet-O-FUW lentiviral vector, and was a kind from Dr. Jason Tchieu (Cincinnati Children's Hospital). Lentiviral transfer vectors were transfected into 293T cells with packaging vector pspax2 (Addgene 12260) and envelop vector vsvg using linear polyethylenimine. Media was changed to MEF media with 20 mM HEPES 4 hours post transfection. Virus-containing media was harvested at 48h and 72h, combined, and filtered through a 0.45 µm PVDF filter. Virus containing media was combined with fresh media at a ratio of 1:1 and 10 µg/ml Hexadimethrine Bromide (polybrene) to transduce target cells.

RNA isolation and library preparation

Reprogramming was initiated in two independent experiment replicate samples, and RNA was isolated from each using TRIzol at the indicated timepoint. One-fifth the volume of chloroform was added and phases were separated by max centrifugation. The upper layer was isolated, RNA was precipitated with 0.53 volumes of ethanol, and applied to a RNeasy column (Qiagen 74104). RNA was washed with 500 µl RW1 and DNA was digested on the column with DNase (Qiagen 79254) for 30 min. RNA was washed according to the RNeasy protocol and eluted in 30 ul of H_2O. RNA was quantitated and 1 µg of each sample was combined with 20 ng of RNA from 293T (human) cells, prepared as above, as a spike-in control for sequencing normalization (timecourse and CDH1 sort studies). The cDNA library was constructed using TruSeq RNA Sample Preparation kit V2 (RS-122-2002) according to the manufacturer's instructions. Libraries were assessed with Qubit and Bioanalyzer3.0.

RNA-Seq computational and statistical analysis

Greater than 40 million reads of timecourse DOT1Li libraries (Fig 1) and CDH1 sort libraries (Fig 4) were sequenced PE150 by Novogene on an Illumina HiSeq 4000. Greater than 25 million reads of CDH1 expression libraries (Fig S4) were sequenced SE100 by the University of Wisconsin Biotechnology Center on a HiSeq 2500. Sequencing quality was assessed with FastQC (http://www.bioinformatics.babraham.ac.uk/projects/fastqc/). Sequenced reads were processed using Trimmomatic (Bolger et al., 2014) with the following parameters: LEADING:3 TRAILING:3 CROP:100 HEADCROP:10 SLIDINGWINDOW:4:15 MINLEN:36. Reads were aligned to the mm9 and hg18 genome using RSEM-1.2.4 (Li and Dewey, 2011) with a mismatch per seed set to 2 and seed length set to 28 (-bowtie-m 200 --bowtie-n 2 --forward-prob 0.5 --seed-length 28 --paired-end). RSEM-1.2.4 alignment yielded transcripts per million (TPM) for each gene. Matrices of TPM of all genes were generated in R and used to assess RNA-Seq replicates. Pearson correlation of replicate samples was performed in R and plotted with the package pheatmap. Classical multidimensional scaling was performed to determine the proportion of variance explained by dimensions with the following parameters:
mds <- cmdscale(dist(PCA_data), k=3, eig=TRUE), mds$eig,
eig_pc <- mds$eig * 100 / sum(mds$eig).
Two dimensions were plotted as over 80% of the data was explained for all analyses using: mds <- cmdscale(dist(PCA_data)). Replicate RNA-Seq sample TPM were averaged for all main figures since they clustered together in both statistical tests.

A matrix of unnormalized reads per replicate mapping to the mouse or human genome was generated with R. Differentially expressed (DE) genes were called with EBSeq (Leng et al., 2013) using the human matrix for normalization (MedianNorm(human_matrix)). Differentially expressed genes were filtered to have a posterior probability DE greater than 0.95 and a 2 or greater posterior fold change (PostFC). Expression changes reported are PostFC values determined by EBSeq unless otherwise noted to be TPM. Cluster3.0 was used to perform k-means clustering of DE genes (de Hoon et al., 2004). Clusters were visualized as Log2 fold change relative to MEF TPM with Java TreeView (Saldanha, 2004). Motif discovery was performed using HOMER Motif Analysis (Heinz et al., 2010) with the following parameters: findMotifs.pl -start -1000 -end 100 -len 6,10. Gene Ontology was performed using HOMER and DAVID (Huang et al., 2009). DAVID parameters included: GOTERM_BP_4 and GOTERM_MF_4, viewed by functional annotation clustering. GO Terms within functional annotation clusters with an enrichment score more than 2 were considered significant. DE genes were compared to a published shRNA iterative screen dataset (Borkent et al., 2016). Fisher's exact test was performed in R.

DOT1L target gene scRNA-seq analysis

Expression of potential DOT1L targets was assessed with single cell RNA-seq data (GEO: GSE108222). Briefly, cells expressing the gene of interest were displayed on a t-distributed Stochastic Neighbor Embedding (t-SNE) cluster plot of MEFs, ESCs, and reprogramming cells in FBS constructed using Monocle2 v2.6.3 on R version 3.4.3 with cells that passed quality control as previously described (Tran et al., 2019).

ChIP-Seq analysis

H3K79me2 ChIP-Seq data with the accession number GSE90895 (Chronis et al., 2017) was downloaded from Gene Expression Omnibus and aligned to mm9 using Bowtie2 (Langmead and Salzberg, 2012) with the default parameters. Sam files were converted into Bam files and sorted with samtools-1.2 (Li et al., 2009) with the default parameters. Peaks were called relative to the input with MACS2 (Zhang et al., 2008) using the following parameters: --broad -p 0.0001. Peak files were annotated using EASeq (Lerdrup et al., 2016) from the center of the peak to the nearest gene center. Genes with peaks were visually mapped back on to the Log10 TPM versus Log2 posterior fold change using R ggplot2 (geom_point graph). Overlaps of DE genes with H3K79me2-modified genes performed with Venny2.1 (https://bioinfogp.cnb.csic.es/tools/venny/). ChIP enrichment was visualized using Integrative Genomics Viewer (IGV) (Robinson et al., 2011).

Immunofluorescence

Coverslips were fixed in 4% paraformaldehyde-PBS, permeabilized in 0.5% Trition-X-PBS, and washed in 0.2% Tween-20-PBS. Coverslips were blocked for 30 min in blocking buffer (1x PBS, 5% donkey serum, 0.2% Tween-20, and 0.2% fish skin gelatin). Cells were stained for 1 hr with primary

antibody in blocking buffer, rinsed 2x in wash buffer, and stained for 1 hr with secondary (1:1000) in blocking buffer. Coverslips were rinsed with wash buffer, stained with DAPI (0.1 µg/ml) in wash buffer, and rinsed with wash buffer. The following antibodies were used for immunofluorescence: anti-murine NANOG (Cosmo Bio RCAB0002P-F, 1:100 and Cell Signaling Technology 8822S, 1:1000), anti-human NANOG (R&D Systems AF1997, 1:100), anti-CDH1 (eBiosciences 14-3249-80, 1:100), and anti-DPPA4 (Thermofisher PA5-47530, 1:100). Colony counts and imaging were performed on Nikon Eclipse Ti using NIS Elements software.

Immunoblot

Whole cells were lysed in RIPA buffer (150 mM NaCl, 1% NP-40, 0.5% Na deoxycholate, 0.1% SDS, 25 mM Tris pH 7.4) with 1x protease inhibitor (Roche 04693116001), sonicated for 5 secs at 20% amplitude, and quantified by cell count or with the DC Protein Assay (BioRad 5000112) according to the manufacturer's instructions. Equal amounts of protein were loaded onto an SDS-Page gel and transferred to a nitrocellulose membrane. Membranes were blocked in blocking buffer (5% milk, 0.1% Tween-20, 1x PBS) followed by incubation with primary antibody in blocking buffer. Membranes were washed 0.1% Tween-20-PBS and incubated with secondary antibody in blocking buffer. Membranes were washed and visualized with ECL reagent. Images were quantified using Image Studio Lite software. Primary antibodies included: anti-H3K79me2 (Abcam ab3594, 1:1000) and anti-α-TUBULIN (Cell Signaling 3873, 1:5000).

Flow cytometry and sorting

For cell cycle determination, cells were fixed in 1 volume of PBS with 9 volume of cold 70% ethanol and permeabilized by freezing at -20 for at least 2 hours. Cells were washed with FACS buffer (1xPBS, 2% FBS, 1mM EDTA), and stained for 30 min in 100 µL FACS buffer containing 1 µL anti-KI-67-Alexa Fluor 488 (BioLegend 151204) per million cells, as previously described (Kim and Sederstrom, 2015). Cells were washed with FACS buffer and DNA was stained for 20 min with 50 µg/ml of propidium iodide (in 1xPBS and 2 mM $MgCl_2$) supplemented with 100 µg/ml RNaseA.

Live cells were used for surface marker staining. Cells were washed in 1x PBS and incubated with antibodies in 1xPBS with 1% FBS for 1 hour. Sorting was performed on a BD FACS AriaII (UW Carbone Cancer Center, Grant #: 1S10RR025483-01) with appropriate controls for gating. FACS quantitation was performed on a BD Accuri C6 Flow Cytometer. Primary antibodies used were anti-THY1-PE (eBioscience 12-0903-81, 1:100) and anti-CDH1-eFluor660 (eBioscience 50-3249-80, 1:100).

siRNA transfection

MEFs were plated at a confluency of 20,000 cells per 24 well on coverslips. Cells were transfected 24 hours after plating with 20 nM siRNA using DharmaFECT1 (Dharmacon T200104) according to the manufacturer's instructions. Reprogramming was initiated immediately using 2 µg/ml of doxycycline with either vehicle (DMSO) control, 5 µM SGC0946/DOT1Li (ApexBio A4167). Cells were transfected every two days during reprogramming, and siRNA was increased to 40 nM at day 4 to account for increased cell number. Knockdown efficiencies were determined 48h after transfection. si*Dot1l* (J-057964-12), si*Hoxd12* (M-046274-01), si*Nfix* (MQ-045912-01), si*Fosl1*(MQ-040704-01) were purchased from Dharmacon Horizon. si*Hic1* (mm.Ri.Hic1.13.1), si*Meox2* (mm.Ri.Meox2.13.1), si*Twist2* (mm.Ri.Twist2.13.1,) were purchased from IDT.

RT-qPCR

RNA was isolated using the Isolate II RNA Mini Kit (Bioline BIO-52072), and 1 µg was converted to cDNA using the qScript cDNA Synthesis Kit (VWR 101414). Technical replicates of 20 ng (based on RNA concentration) were used to measure Ct on a BioRad CFX96 thermocycler with iTaq UniverSYBR Green SMX (BioRad 1725125) in 10 µl reactions. Relative expression was calculated against the geometric mean of two housekeeping genes. Hierarchical clustering of relative expression values performed with Cluster3.0 (de Hoon et al., 2004) using the uncentered correlation similarity metric and the average linkage clustering method. Primers used in this study:

Gene	Forward 5'-3'	Reverse 5'-3'
Bex1	TGGTGGTGAGCATCTCTAGAAAGAG	TAGAAGCTGGTAACAGGGAG

Cd5l	AGGTGATCTGCACAGACTTTGAT	TTGAGGTGATTATGGGGGCG
Cdh1	GCCACCAGATGATGATACCC	GGAGCCACATCATTTCGAGT
Dot1l	GCGGCTGTGTGACAAATACA	CCATACACCTCAGGGGAGAA
Dsc2	AGGGCCCAGTAGAGGTACTA	GTGGGAAGGGACCCAATGAA
Egfl6	CTGCAGTGTTCTGTGATCCCT	CTTCATGGTGCGCTTGTGAG
Epcam	CATTTGCTCCAAACTGGCGT	TTGTTCTGGATCGCCCCTTC
Fabp4	CATAACCCTAGATGGCGGGG	CGCCTTTCATAACACATTCCACC
Fosl1	CGGCCAGGAGTCATACGAG	CCTTTCTTCGGTTTCTGCAC
Hic1	GAGCTTTGGTGACAACCTGTA	CTGCCATATAACGCCTCTTCTT
Hoxd12	CTCTTGCCTGCGATCTTCACT	GAATTCATTGACCAGGAATTCGTT
Klhl30	CGCCCAAGTATGTCAGCAAC	TGACACTCCACGCATCTGTC
Krt18	AATCGAGGCACTCAAGGAAGAA	GGCATCCACTTCCACAGTCA
Meox2	TGCGCACCAGGGGATTATG	TGGGAATCTGAGCTGTCGC
hMEOX2	AGACTGAGGCGATACGAGATAG	CCTTTACCCTCTTCCACTTCATC
Nanog	CATCCCGAGAACTATTCTTGCT	GAGGCAGGTCTTCAGAGGAA
hNANOG	CAGCTGTGTGTACTCAATGATAGATTT	CAACTGGCCGAAGAATAGCAATGGTGT
Nfix	CATCAGGGCCCAACTTCTCA	CTTGGTGCTGCTGGTGGAA
hNFIX	GAGTCCCAGCTACTACAACATC	GCTCTCCATCTCACTGTCATC
Sall4	AACATATGCGGGCGGGCCTTCA	CCAGGAGGCGGGGTCCACACTC
Tcfap2c	GGGCTTTTCTCTCTTGGCTGGT	TCCACACGTCACCCACACAA
Twist2	CGCTACAGCAAGAAATCGAGC	GCTGAGCTTGTCAGAGGGG
Gapdh	TTCACCACCATGGAGAAGGC	CCCTTTTGGCTCCACCCT
β-actin	TGTTACCAACTGGGACGACA	TCTCAGCTGTGGTGGTGAAG

SUPPLEMENTAL REFERENCES

Bolger, A.M., Lohse, M., and Usadel, B. (2014). Trimmomatic: a flexible trimmer for Illumina sequence data. Bioinformatics *30*, 2114–2120.

Borkent, M., Bennett, B.D., Lackford, B., Bar-Nur, O., Brumbaugh, J., Wang, L., Du, Y., Fargo, D.C., Apostolou, E., Cheloufi, S., et al. (2016). A Serial shRNA Screen for Roadblocks to Reprogramming Identifies the Protein Modifier SUMO2. Stem Cell Reports *6*, 704–716.

Chronis, C., Fiziev, P., Papp, B., Butz, S., Bonora, G., Sabri, S., Ernst, J., and Plath, K. (2017). Cooperative Binding of Transcription Factors Orchestrates Reprogramming. Cell *168*, 442-459.e20.

Heinz, S., Benner, C., Spann, N., Bertolino, E., Lin, Y.C., Laslo, P., Cheng, J.X., Murre, C., Singh, H., and Glass, C.K. (2010). Simple combinations of lineage-determining transcription factors prime cis-regulatory elements required for macrophage and B cell identities. Mol. Cell *38*, 576–589.

de Hoon, M.J.L., Imoto, S., Nolan, J., and Miyano, S. (2004). Open source clustering software. Bioinformatics *20*, 1453–1454.

Huang, D.W., Sherman, B.T., and Lempicki, R.A. (2009). Systematic and integrative analysis of large gene lists using DAVID bioinformatics resources. Nat Protoc *4*, 44–57.

Kim, K.H., and Sederstrom, J.M. (2015). Assaying Cell Cycle Status Using Flow Cytometry. Curr Protoc Mol Biol *111*, 28.6.1-11.

Langmead, B., and Salzberg, S.L. (2012). Fast gapped-read alignment with Bowtie 2. Nat Methods *9*, 357–359.

Leng, N., Dawson, J.A., Thomson, J.A., Ruotti, V., Rissman, A.I., Smits, B.M.G., Haag, J.D., Gould, M.N., Stewart, R.M., and Kendziorski, C. (2013). EBSeq: an empirical Bayes hierarchical model for inference in RNA-seq experiments. Bioinformatics *29*, 1035–1043.

Lerdrup, M., Johansen, J.V., Agrawal-Singh, S., and Hansen, K. (2016). An interactive environment for agile analysis and visualization of ChIP-sequencing data. Nat. Struct. Mol. Biol. *23*, 349–357.

Li, B., and Dewey, C.N. (2011). RSEM: accurate transcript quantification from RNA-Seq data with or without a reference genome. BMC Bioinformatics *12*, 323.

Li, H., Handsaker, B., Wysoker, A., Fennell, T., Ruan, J., Homer, N., Marth, G., Abecasis, G., Durbin, R., and 1000 Genome Project Data Processing Subgroup (2009). The Sequence Alignment/Map format and SAMtools. Bioinformatics *25*, 2078–2079.

Robinson, J.T., Thorvaldsdóttir, H., Winckler, W., Guttman, M., Lander, E.S., Getz, G., and Mesirov, J.P. (2011). Integrative genomics viewer. Nat Biotechnol *29*, 24–26.

Saldanha, A.J. (2004). Java Treeview--extensible visualization of microarray data. Bioinformatics *20*, 3246–3248.

Tran, K.A., Pietrzak, S.J., Zaidan, N.Z., Siahpirani, A.F., McCalla, S.G., Zhou, A.S., Iyer, G., Roy, S., and Sridharan, R. (2019). Defining Reprogramming Checkpoints from Single-Cell Analyses of Induced Pluripotency. Cell Rep *27*, 1726-1741.e5.

Zhang, Y., Liu, T., Meyer, C.A., Eeckhoute, J., Johnson, D.S., Bernstein, B.E., Nusbaum, C., Myers, R.M., Brown, M., Li, W., et al. (2008). Model-based analysis of ChIP-Seq (MACS). Genome Biol *9*, R137.